Strong Plasma Acceleration by Slow Shocks Resulting from Magnetic Reconnection

Tetsuya Sato*

Plasma Physics Laboratory, Princeton University

Princeton, New Jersey 08544

An externally-driven magnetic reconnection is simulated for two two-dimensional magnetohydrodynamic models with anomalous resistivity. A closed boundary model where an O-type neutral point is formed between two X-type neutral points; and an open-ended model where only an X-type neutral point is formed. Computer runs have shown that: (1) X-shaped (Petschek type) slow shocks are formed. Upon examination of their fine structure, it is found that the Rankine-Hugoniot shock conditions are extremely well satisfied. (2) In the closed boundary case, the plasmas entering into the magnetic island through the X-type neutral points are moderately accelerated along the magnetic island boundaries. Two pairs of vortices are formed internally in such a way that the plasmas are confined. Consequently, the region of the island expands as the pressure increases. As reconnection proceeds, another set of vortices is generated in the expanding island causing the plasma to become

turbulent. (3) In the open-ended case, the plasma acceleration is intensified and strong jet streams are generated on the downstream side of the slow shocks, with the speed approaching the Alfvén speed of the upstream region. Interestingly, the jet streams tend to concentrate preferentially along the plasma sheet boundaries (shock fronts). This is attributed to sharp pressure gradients along the magnetic field lines as a result of slow shocks whose fronts obliquely intersect the field lines. These features of strong jetting of plasmas along the plasma sheet boundaries can explain the recent observations of high velocity proton flows in the Earth's magnetotail during substorm expansions. (4) Examination of the energy conversion rate has shown that the exernally-driven magnetic reconnection acts as a powerful magnetic energy converter.

*Permanent Address: Geophysical Research Laboratory, University of Tokyo, Tokyo 113, Japan.

INTRODUCTION

Cosmical plasmas, and laboratory plasmas as well, are often immersed in magnetic fields, and in many practical cases they can be considered to be collisionless and dissipationless, so that the "frozen-in" principle is applicable. According to this principle, plasmas that have origins at different places can be neither mixed up nor fused into one. In other words, every star and planet with its own magnetized plasma would always be isolated, and would not directly interfere with each other. Likewise, plasmas that initially reside in regions separated by rational surfaces in tokamaks would never be mixed up. If this is always the case, then human beings on earth would never see auroras, and tokamak plasmas would never undergo violent disruptions. In reality, however, something must happen to violate the frozen-in condition on a contact point or surface of two plasmas with different origins. "Anomalous transport" may be the most efficient and important process violating the frozen-in condition.

Let us examine two well-known mechanisms of anomalous viscosity and anomalous resistivity. The Axford-Hines hypothesis [1961] states that a viscous-like interaction must take place on the dayside magnetopause. Anomalous resistivity can also play an essential role in violating the frozen-in principle and in merging different magnetized plasmas as stated by Dungey's magnetic reconnection hypothesis [1961]. As one potential candidate of causing an explosive energy release such as a magnetospheric substorm and a solar flare, magnetic reconnection has long attracted the attention of space physicists. Recently, the magnetic reconnection process has been discussed as a likely mechanism leading to the major disruption in tokamaks [see

White et al., 1977].

Because of the mathematical difficulty, however, earlier works deal primarily with steady state reconnection [see Petschek, 1964; Sonnerup, 1970; Yeh and Axford, 1970; Vasyliunas, 1975; and Priest, 1973]. Recently Hayashi and Sato [1978] and Sato and Hayashi [1979] have developed a numerical MHD model of an externally driven reconnection that may be able to represent magnetic reconnection in the magnetotail. The main conclusions obtained by these simulations are as follows: (1) As soon as anomalous resistivity is generated in a local region of the neutral sheet, reconnection develops and the magnetic energy stored prior to reconnection is rapidly converted into the plasma bulk flow. (2) Strong plasma acceleration appears to be closely related to the shock-like structure formed downstream of the magnetic separatrix and also partly to fast mode expansion in the upstream region. (3) The speed of the outflowing plasmas becomes as high as the Alfvén speed in the upstream region. These results seem to provide support for the idea that magnetic reconnection can be a primary energy source of magnetospheric substorms.

The Sato-Hayashi model [1979] assumed that the output plasma could freely exit from the system; in other words, an open-ended system was considered. The anomalous resistivity adopted was assumed to be a direct function of the neutral sheet current. As can be seen in the sketch given in Fig. 1, which illustrates what is happening in the magnetotail [see Russell and McPherron, 1973; Hones et al., 1974; Schindler, 1974; Terasawa and Nishida, 1976; Hones, 1977], it appears that in the early phase of reconnection earthwardly-accelerated plasmas would be impeded by the rigid earth's

dipole field and tailwardly accelerated plasmas would be trapped in a magnetic island. Accordingly, we postulate that magnetic reconnection proceeds in a bounded state for a while until the energized, confined region becomes unstable, and the energy of the trapped plasma is suddenly released down into the ionosphere by some mechanism, that is, until the onset of auroral breakup. On the tailside of the reconnection line, an O-type magnetic loop would be formed [Stern, 1979] and the particles trapped therein would eventually be ejected far downstream to merge into the solar wind.

From these considerations, we first simulate a magnetic reconnection process that occurs in a closed system and then compare the result with the process occurring in an open-ended system. Although more attention is directed toward the space plasma in this paper, we expect that our simulations also will provide some ideas about the reconnection process in laboratory plasmas.

There is an observational evidence that the plasma sheet thins prior to a substorm in a relatively near earth region of the magnetotail [Pytte and West, 1978]. The evidence suggests that an additional pressure must be applied to the plasma sheet boundary before a substorm. Similarly, magnetic field measurements in the lobe region of the magnetotail indicate that there is an energy build-up stage prior to a substorm [Fairfield and Ness, 1970; Maezawa, 1975]. These observational facts are self explanatory if we admit that magnetic reconnection is taking place on the dayside magnetopause in accordance with the southward turning of the interplanetary magnetic field [see Nishida, 1978]. Indeed, once the dayside magnetosphere is eroded by magnetic reconnection [Aubry et al., 1970], the solar wind plasma invades the magnetosphere [Shelley et al., 1978; Schopke et al., 1976] and ends up with a compression of the plasma sheet.

Judging from the nonuniformity of the magnetotail configuration, the invading solar wind plasma would not uniformally compress the plasma sheet throughout the tail region, but would intensively compress a certain weak region of the plasma sheet. Since the deformation of the plasma sheet due to the solar wind invasion is not yet solved, one cannot answer at present where the weak point of the plasma sheet is located. Nevertheless, from the satellite observations, it appears that the weak point is located somewhere around $-20R_E < X < -10R_E$, where reconnection would first take place [Pytte and West, 1978; Nishida and Nagayama, 1973; Pytte et al., 1976, see Nishida, 1978].

Therefore, we postulate that reconnection in the tail is triggered by a local compression of the plasma sheet as a result of an invasion of the solar wind into the magnetotail; we postulate that reconnection can be triggered by an external force. It is also likely in tokamaks that reconnection is triggered by a plasma motion resulting from a kink instability.

There is another important factor in simulating magnetic reconnection in the MHD regime, i.e., the resistivity. The classical resistivity in space is astonishingly small except for a thin transition layer between the neutral atmosphere and the fully ionized space. In order to liberate the magnetic energy in a reasonably fast time scale, some sort of anomalous dissipation is required. In our model, which assumes a local compression of the plasma sheet (or neutral sheet) by an external flow, the plasma sheet suffers a thinning. This implies an increase in the neutral sheet current and, hence, in the relative diamagnetic drift velocity between the electrons and ions in the neutral sheet. Thus one may expect that some plasma

instability would result in limiting the ever-increasing neutral current; i.e., an anomalous resistivity would arise. Anomalous resistivity associated with plasma instabilities in the neutral sheet have been discussed by several authors [Smith and Priest, 1972; Smith, 1977; Coroniti and Eviator, 1977; Huba et al., 1977]. In the magnetosphere the lower-hybrid-drift instability seems to be the most viable candidate [Huba et al., 1978; Papadopoulos, 1979]. Davidson and Gladd [1975] have given a formula for anomalous resistivity associated with the lower-hybrid-drift instability which is proportional to the square of the drift velocity in the neutral sheet. Accordingly, we presume that a local compression of the plasma sheet ends up with a generation of a certain anomalous resistivity that is proportional to the square of the drift velocity in the neutral sheet.

Preliminary results are given in the paper by Sato et al. [1978]. In this paper the details and the extended results of an externally-driven reconnection for the closed and open-ended systems will be presented, with particular emphasis on the energetics, the generation of strong parallel plasma flows, and the structure of slow shocks.

Magnetic field observations by satellites have provided some circumstantial support for the occurrence of magnetic reconnection in the magnetotail in association with magnetospheric substorms [see Nishida, 1978 and references cited]. Because of the coarse-grained observations, however, it is hard from the satellite observations alone to conclude that magnetic reconnection is ctually taking place in the magnetotail [Liu et al., 1977]. Meanwhile, we are now able to measure the plasma bulk flow in the magnetotail. Above all, the finding of strong jetting of protons in the magnetotail provides

us with an important and significant clue in the understanding of the magnetospheric dynamics [Hones et al., 1976; Hones, 1976; Frank and Ackerson, 1976; Liu et al , 1977; Krimigis and Sarris, 1979]. Although controversial points remain in the interpretation of data [Hones, 1979], one ought to elucidate the elementary process of producing such strong jetting of plasmas in the magnetotail.

The primary purpose here is then to demonstrate how the strong jetting of plasmas arises as a result of magnetic reconnection, and to see whether magnetic reconnection can indeed be a primary energy source of magnetospheric substorms. The parameters to be adopted in the simulations are not necessarily real. But the results obtained should give some progress in the comprehension of magnetospheric substorms and solar flares and also of the disruption mechanism in tokamaks.

NUMERICAL MODELS

The equations to be solved are a set of two-dimensional magnetohydrodynamic equations:

$$\frac{\partial \rho}{\partial t} = -\nabla \cdot \rho \mathbf{v} \quad , \tag{1}$$

$$\frac{\partial \rho \mathbf{v}}{\partial t} = -\nabla \cdot \left(\rho \mathbf{v}\mathbf{v} + \frac{1}{\mu_o} \mathbf{B}\mathbf{B} \right) - \nabla \left(p - \frac{B^2}{2\mu_o} \right) \quad , \tag{2}$$

$$\frac{\partial \mathbf{B}}{\partial t} = \nabla \times (\mathbf{v} \times \mathbf{B}) - \nabla \times (\eta \mathbf{j}) \quad , \tag{3}$$

$$\frac{\partial U}{\partial t} = -\nabla \cdot \mathbf{S} \tag{4}$$

with

$$\underset{\sim}{j} = \nabla \times \underset{\sim}{B}/\mu_o \quad ,$$

$$U = \rho v^2/2 + p + B^2/2\mu_o \quad ,$$

$$\underset{\sim}{S} = (U + p + B^2/2\mu_o)\underset{\sim}{v} - (\underset{\sim}{v}\times\underset{\sim}{B})\underset{\sim}{B}/\mu_o + \eta \underset{\sim}{j} \times \underset{\sim}{B}/\mu_o$$

where η is the resistivity, and the other notations are conventional; the ratio of the specific heats is taken to be 2.

Referring to the theory of Davidson and Gladd for a lower-hybrid-drift instability [1975], we assume the anomalous resistivity to take the following form:

$$\eta = \begin{cases} \alpha(V_d - V_c)^2 & \text{for } V_d > V_c \\ 0 & \text{otherwise} \end{cases} \qquad (5)$$

where V_d is the diamagnetic (mostly ion) drift velocity given by $V_d = j/ne$, j being the neutral sheet current, n being the plasma density and e being the electronic charge; α and V_c are arbitrary constants which are externally given. Of course, this is a model of anomalous resistivity which ought to be justified by a kinetic treatment. But at least under the assumption that the resistivity is dependent on a macroscopic quantity of the medium, such as the diamagnetic drift velocity, it has been proved that the choice of the functional form of the resistivity, $\alpha|j/ne - V_c|$ or $\alpha|j/ne - V_c|^3$, makes no essential difference in the reconnection process [Sato and Hayashi, 1979]. Thus, the choice of such a specific functional form as Eq. (5) may not leave any serious problems.

The initial plasma configuration is taken to be as follows:

$$\underset{\sim}{B} = B_o \hat{\underset{\sim}{x}} \tan(z/L) \qquad \text{(magnetic field)}$$

$$\underset{\sim}{j} = j_o \hat{\underset{\sim}{y}} \operatorname{sech}^2(z/L) \qquad \text{(electric current)}$$

$$p = p_o \operatorname{sech}^2(z/L) \qquad \text{(pressure)}$$

$$\rho = \rho_o \qquad \text{(mass density)}$$

$$\underset{\sim}{v} = 0 \qquad \text{(velocity)} \qquad (6)$$

where $\hat{\underset{\sim}{x}}$ and $\hat{\underset{\sim}{y}}$ are the unit vectors along the x and y axes, respectively; x,y and z construct right-handed Cartesian coordinates; B_o, j_o, p_o, and ρ_o are all constants and $j_o = B_o/\mu_o L$ and $p_o = B_o^2/2\mu_o$ hold.

In the actual calculations all variables are normalized to the following parameters: L(length), $V_A \equiv B_o/(\mu_o \rho_o)^{1/2}$ (velocity), B_o (magnetic field), ρ_o (mass density), $B_o/\mu_o L$ (current), $B_o^2/2\mu_o$ (pressure), B_o^2/μ_o (energy), $\mu_o L V_A$ (resistivity), and $B_o V_A$ (electric field).

Calculations are made on a rectangular box surrounded by $x = \pm 3$ and $z = \pm 2$. Since the unit length corresponds roughly to a half of the plasma sheet ($\sim 3R_E$ in the magnetosphere), it may be considered that this covers roughly $6R_E$ in the Z_{SM} axis and $10R_E$ in the X_{SM} axis in the solar magnetospheric coordinate system. With regards to this numerical scheme, it should be noted that the paper by Sato and Hayashi [1979] has verified that the scheme is sufficient to elucidate the physical process of reconnection and that the position of the boundaries does not affect the result.

At T(normalized time) = 0 we start to inject plasmas from the boundaries at $z = \pm 2$ (hereafter we call them the in ut boundaries) in such a way that the mass, magnetic energy and total energy fluxes perpendicular to the magnetic field at the boundaries are conserved. Note, however, for a short initial period ($0 \leq T \leq 2$) the fluxes are monotonically increased to avoid a numerical instability and are fixed to constant values, thereafter.

The injection flux pattern on the input boundaries, F(x), is chosen in the following way for the closed reconnection model:

$$F(x) = \begin{cases} A_o & \text{for } x_2 \leq x \leq 3 \\ \frac{A_o}{2}\left(1 + \cos \frac{(x_2 - x)}{(x_2 - x_1)}\pi\right) & \text{for } x_1 \leq x \leq x_2 \\ 0 & \text{for } 0 \leq x \leq x_1 \end{cases} \qquad (7)$$

and $F(x) = F(-x)$ where $x_1 = 0.1$, $x_2 = 32/37$ and A_o is a parameter that gives the strength of the inflow plasma flux.

On the side boundaries at $x = \pm 3$ we have imposed the following conditions:

$$B_z = 0 \quad , \quad v_x = 0 \quad , \qquad (8)$$

These conditions ensure that the plasma convection is confined within the rectangular box surrounded by $x = \pm 3$ and $z = \pm 2$.

The two-step Lax-Wendroff method is employed and the calculation is performed in only one quadrant of $0 \leq x \leq 3$ and $0 \leq z \leq 2$, which are divided into 74 x 83 grids with equal intervals in each direction. Details of the numerical procedure are given in

the paper by Sato and Hayashi [1979]

For the open-ended reconnection model, the injection flux pattern on the input boundaries, F(x), is taken to be

$$F(x) = \begin{cases} A_o & \text{for } 0 \le x \le x_1 \\ \frac{A_o}{2}\left(1 + \cos\frac{(x-x_1)}{3-x_1}\pi\right) & \text{for } x_1 \le x \le 3 \end{cases} \qquad (9)$$

and $F(x) = F(-x)$ where $x_1 = 0.1$. The boundary conditions on the sides at $x = \pm 3$ are designed so that plasmas and waves can freely exit and enter the system through them.

RESULTS FOR CONFINED RECONNECTION

Runs for the closed system are performed for the following two cases: (i) $A_o = 0.2$, $V_c = 3.0$, $\alpha = 0.02$, and (ii) $A_o = 0.05$, $V_c = 3.0$, $\alpha = 0.02$. Before going into the description of the results, we shall briefly comment on the relationship between the above parameters and the magnetospheric parameters.

We take the Alfvén speed (V_A) in the magnetospheric lobe to be $V_A = 500$ km/s and the electron (T_e) and proton (T_i) temperatures in the plasma sheet to be $T_e = 1$ keV and $T_i = 5$ keV; hence, v_{te} (electron thermal velocity) $\approx 1.3 \times 10^4$ km/s and v_{ti} (proton thermal velocity) $\approx 7.1 \times 10^2$ km/s. Therefore, $A_o = 0.2$ and $A_o = 0.05$ imply that the initial velocity of the inflow plasma through the input boundaries corresponds, respectively to 100 km/s and 25 km/s. These velocities are quite conceivable when we consider the invasion of the solar wind plasma from the dayside magnetosphere. If we take the unit length to be 15000 km, then the unit time corresponds to 30 secs.

The threshold diamagnetic drift velocity for the occurrence of a plasma instability, presumably a lower-hybrid-drift instability (namely, $V_c = 3$), corresponds to 1500 km/s. Obviously, this velocity is much smaller than the electron thermal velocity but is comparable to the ion thermal velocity. As inferred from previous simulations [Sato and Hayashi, 1979], the choice of V_c, say $V_c = 3$ or $V_c = 1$ is not essential in the development of reconnection. Actually, the diamagnetic velocity starts to increase from $V_d = 1$, therefore, we may expect that a kinetic lower-hybrid-drift instability will arise at first in the actual case [consult Huba et al., 1977].

The parameter α gives the strength of the anomalous resistivity. Let us examine the resistivity in terms of the magnetic Reynold's number R_M. By using the normalized quantities, the Reynold's number is written as $R_M = V\ell/\alpha(V_d - V_c)^2$ for $V_d > V_c$ and infinite for $V_d \leq V_c$ where V is the normalized plasma flow velocity in the x-z plane and ℓ is the normalized characteristic length of the magnetic field. Before the diamagnetic drift velocity V_d reaches the threshold, R_M is infinite everywhere, but it decreases from infinity as the diamagnetic velocity increases wherever the velocity exceeds the threshold. Let us get a rough idea of how small the magnetic Reynold's number can become during the process of reconnection. The number is a function of the position in the x-z plane. As will be discussed later, it becomes finite only in the vicinity of the X-type neutral point and in a very narrow region within the X-type slow shock layers. The minimum of R_M may be at the X-type neutral point where $(V_d - V_c)$ is at most 1 and typically 0.5. Since $V \sim 1$, $\ell \sim 1$, and $\alpha = 0.02$, the minimum Reynold's number in our simulations is 2×10^2. Of course, this value may be too small in the actual magnetotail and in

laboratories even if an anomalous resistivity is taken into consideration. As was previously ...ved [Sato and Hayashi, 1979], however, the choice of α is not so sensitive to the development of reconnection. From these considerations it may be said that the present simulation can provide us with important, qualitative and quantitative clues as to the externally-driven magnetic reconnection, in particular as to whether magnetic reconnection can be a primary energy source of magnetospheric substorms or not.

Let us now go on to describe the numerical result of case (1). Figure 2 shows the temporal evolution of the equicontours of the vector potential (magnetic flux surfaces). As can be seen from Eq. (6), the plasma inflow flux through the input boundaries is maximized at both ends ($x = \pm 3$) at the top and bottom boundaries ($z = \pm 2$). Therefore, the initially anti-parallel magnetic field lines are pushed toward the neutral sheet around $x = \pm 3$ and the diamagnetic drift increases around $x = \pm 3$ on the neutral line. As this condition continues and the anomalous resistivity appears, the magnetic field lines start to be reconnected (see the bottom-left panel of Fig. 2) at $x = \pm 3$ and $z = 0$ and an O-type neutral point is formed at the middle point. As time elapses, it is seen that the magnetic island grows and expands.

Figure 3 shows a time series of the plasma flow pattern corresponding to that of the magnetic field topologies of Fig. 2. The top panel may be understood to exhibit the pattern of plasma inflow. The first three panels ($T = 1.0$, 5.0, and 10.0) exhibit the flow patterns during the initial phase before reconnection takes place. In the early phase of the reconnection development, four symmetric,

weak convection cells (vortices) develop in such a way that the plasma entering the magnetic island through the magnetic separatrix convects away from the island and merges into the inflow plasma. Thus the flow pattern is similar to the tearing mode flow pattern (see the top-right panel). As further reconnection develops, the flow pattern is seen to be almost reversed in a short period. More interestingly, in accordance with the flow pattern change, the plasma is seen to be rapidly accelerated near the X-type neutral points up to roughly a half of the Alfvén speed in the upstream region, and the jet stream bifurcates along the magnetic island boundaries. The bifurcated jet streams then turn their directions near the x axis so as to be rolled up inside the magnetic island. As time elapses and the magnetic island expands, the flow pattern is, as a whole, reversed, but two new pairs of vortices are generated near the neutral line ($x \approx \pm 1$ and $z = 0$) and the original pairs of vortices are pushed away from the neutral line. Since the abrupt flow pattern change seems to be pertinent to the evolution of the plasma flow in the magnetic island, let us examine the fine structure of the flow pattern change, as shown in Fig. 4. The time interval of the successive pictures is one in normalized units. At $T = 17.0$ one can notice a slight indication of the birth of two new pairs of vortices near the neutral line, i.e., $x \approx \pm 1$ and $z \approx 0$. The infant vortices grow with time and develop into two pairs of convection cells whose directions are opposite to those of the original tearing mode-type convection cells [see the panels corresponding to $T = 17, 18, 19,$ and 20]. Of particular interest is that young convection cells push out the original cells, forming strong jet streams

on the boundaries between the old and new cells, with the old ones apparently disappearing [see the last panel]. Thus, comparing the first and last panels (T = 16 and 21), one can state that the flow pattern is found to be reversed in a short period. Though not shown here, as time goes futher, newer convection cells whose flow directions are again opposite to those of the previous cells are generated close to the birth places of the previous ones, i.e., at $x \approx \pm 1$ and $z \approx 0$. Again, the younger ones tend to push out the older ones [there is a slight indication of this in the last panel of Fig. 3]. Since the run was cut at $T = 29$, it cannot give a definite conclusion, but it appears that the process repeats and many convection cells are formed inside the island, thus resulting in turbulence.

Figure 5 shows the 3-D graphic displays of the pressure distribution change (left column) and the current distribution change (right column). The top panels represent their initial distributions. The left panels show that the plasma is initially compressed around $x \approx \pm 3$ on the neutral sheet (x axis) by fast MHD modes that propagate toward the neutral sheet as a result of the plasma injection through the input boundaries [see the second panel]. As reconnection proceeds, the magnetic island expands and the pressure in it increases [see the last two panels]. This expansion of "the plasma island" can be attributed to a result of the formation of strong convection cells that swallow up the external plasma as seen in the last two panels of Fig. 4.

The right panels show the corresponding changes of the neutral sheet current. Corresponding to the initial plasma compression by the fast mode, the neutral sheet current is also intensified in the early phase around $x \approx \pm 3$ and $z \approx 0$. With the passage of time,

however, two current layers develop at the plasma sheet boundaries [see the last two panels]. In later discussions, the current layers will be identified as slow shocks.

Figure 6 shows the contour maps of the pressure (top), temperature (middle) and density (bottom) at T = 25 when reconnection has sufficiently developed. Comparison of these panels indicates that the pressure increase (in the middle of the plasma island) is shared equally by the temperature and density increases, this suggesting an adiabatic compression. Another feature of this figure is an appreciable density decrease near the X-type neutral points (x = ±3 and z=0), which is presumably attributed to the abrupt plasma acceleration near the neutral points.

We have made another run for the same confined geometry but with a weaker plasma influx through the input boundaries for case (ii). The magnetic field line topologies (left) and the plasma flow patterns (right) at two different times for this run are shown in Fig. 7. One can immediately notice a convection pattern change exactly the same as in the previous case. The current distributions, at the same time as those of Fig. 7, are shown in Fig. 8, which again show weak slow shocks. Thus the observed results may be considered to be intrinsic to the confined reconnection process.

RESULTS FOR OPEN-ENDED RECONNECTION

If the system is closed permanently, the bulk flow energy converted from the magnetic energy must eventually be converted into thermal energy. The expansion of the magnetic island observed in the previous case was a result of such an adiabatic energy conversion. In both space and laboratory plasmas, the continued expansion of the island must end up with disruption of the plasma. In a laboratory, the plasma would blow up when the magnetic island expands up to the wall, and in space, the energized, trapped plasmas would become unstable sooner or later to release the trapped energy along the field lines connecting to a weakly ionized plasma. Auroral breakups and solar radio bursts may be considered to be results of such instabilities.

Simulation results in the previous section have shown that jetting of plasma arises along a narrow region of the expanding plasma sheet (magnetic island) boundary. Such jetting along the magnetic field (usually mirror field) may produce a parallel electric field whereby electrons are accelerated away from the trapped region. Thus, the next step may be to simulate a case in which the accelerated plasma can freely flow out of the system, namely the open-ended reconnection.

The parameter values are chosen to be the same as those of case (i), i.e., $A_0 = 0.2$, $V_c = 3$, and $\alpha = 0.02$. The side boundaries ($x = \pm 3$) are designed to be free boundaries [see Sato and Hayashi, 1979] and the inflow pattern through the input boundaries is given by (8).

Figure 9 shows a time series of the magnetic field lines and Fig. 10 shows the corresponding plasma flow vectors. The top panel

of Fig. 10 gives an idea of the incoming plasma flow pattern through the input boundaries and the middle-left panel shows a natural outflow pattern through the side boundaries which occurs as a result of fast mode compression at the center where no reconnection takes place. At the bottom-left panel of Fig. 10, it is clearly seen that reconnection has already started at this time (T = 10) and the outgoing plasma begins to be accelerated. The right panels of Figs. 9 and 10 show that as reconnection proceeds, the plasma acceleration is markedly enhanced in the downstream region of the magnetic separatrix and reconnected field lines are conveyed away from the neutral point.

Two additional important conclusions can be drawn from simulation. The first is the development of a fast mode expansion in the upstream region [Sato and Hayashi, 1979]. As is evident by comparing the flow patterns at T = 10 and 15, the streamlines tend to converge toward the X-type neutral point and make a sudden change at the place of slow shocks that will be discussed in detail later [see the upper-right panel of Fig. 10]. The close examination of the magnetic field and the plasma pressure distribution in the upstream region indicates that both the magnetic field and the pressure decrease toward the slow shocks from the input boundaries [see the top-right panel of Fig. 9 and the top panel of Fig. 12]. Thus, the converging character of the streamlines is understood as an indication of a fast mode expansion [see a review paper by Vasyliunas, 1973]. Therefore, it is said that the rapid acceleration in the downstream region is at least partly promoted by this fast mode acceleration in the upstream region.

The second important conclusion is the fact that the plasma is accelerated more preferentially along the magnetic field lines (along the plasma sheet boundaries) than across them in the slow shock region [see the top panel of Fig. 12 and the bottom panel of Fig. 11]. It should be particularly noted that the accelerated velocity reaches the Alfvén velocity of the upstream region (the arrow shown on the right shoulder of the first panel of Fig. 10 gives the scale of the Alfvén speed). Not only the strong proton flows observed in the magnetotail [see for example Hones, 1976; Frank and Ackerson, 1976; Liu et al., 1977; Krimigis and Sarris, 1979] can be well explained, but the present result (occurrence of strong jetting of plasmas along the magnetic field) strongly suggests that this mechanism could be a primary energy source of auroral breakups.

Figure 11 gives a 3-D graphic displays of the sheet currents at three different times. The top and bottom ends of each graph correspond to the size boundaries and the left and right ends correspond to the input boundaries. It is seen from this series of current patterns that the current peaking initially occurs at the neutral sheet due to the fast mode compression [see the top graph] but that with the passage of time the current sheet is separated into two sheets [see the middle graph] and the two sheets develop into sharply peaked layers. The positions coincide with the demarcation zone between the accelerated and nonaccelerated flows in Fig. 10. Figure 12 shows the equicontours of the pressure (top), the temperature (middle), and the density (bottom) at $T = 19$ when reconnection has sufficiently developed. The pressure contours show that a plasma

sheet with sharp boundaries is formed, which is thinned near the X-type neutral point and expands out away from the point. Examination of the positions of the plasma sheet boundaries, the current peakings and the plasma flow singularities leads to the conclusion that all these positions are coincident. All these features indicate that the pecularities must be of slow shocks. Since this is a key conclusion in the present simulation results, we shall give its quantitative proof in the following section.

The middle panel of Fig. 12 shows that the plasma is heated near the X-type neutral point to a considerable degree. In the present simulation, however, the heat conduction is omitted because the anomalous heat conduction rate is not known. The heat will be quickly transported away from the neutral point region because of its high parallel conductivity, so that the temperature gradient will be broadened The bottom panel of the density contours indicates that the plasma is considerably rarefied near the neutral point, as a result, presumably, of fast plasma evacuation due to the rapid outward acceleration.

RANKINE-HUGONIOT RELATIONS IN SLOW SHOCKS

From Eqs. (1 - 4), it is known that the following quantities should be conserved across the shock front; namely, $[B_\perp]$, $[\rho v_\perp]$, $[(\underset{\sim}{v} \times \underset{\sim}{B})_\perp]$, $[\rho v_\perp^2 + p + B^2/2\mu_o]$, and $[(\rho v^2/2 + 2p + B^2/\mu_o)v_\perp - (\underset{\sim}{v}\cdot\underset{\sim}{B}/\mu_o)B_\perp]$, where the subscript "$\perp$" is perpendicular to the shock front. Rewriting the above shock jump conditions in terms of the corresponding normalized quantities, yields

$$[1] \quad B_{1\perp} = B_{2\perp}$$

$$[2] \quad \rho_1 v_{1\perp} = \rho_2 v_{2\perp}$$

$$[3] \quad v_{1\perp} B_{1\parallel} - v_{2\parallel} B_{1\perp} = v_{2\perp} B_{2\parallel} - v_{2\parallel} B_{2\perp}$$

$$[4] \quad 2\rho_1 v_{1\perp}^2 + p_1 + B_{1\parallel}^2 = 2\rho_2 v_{2\perp}^2 + p_2 + B_{2\parallel}^2$$

$$[5] \quad [\rho_1 (v_{1\perp}^2 + v_{1\parallel}^2) + 2p_1 + 2B_{1\parallel}^2] v_{1\perp} - 2(v_{1\parallel} B_{1\parallel} + v_{1\perp} B_{2\perp}) B_{1\perp}$$

$$= [\rho_2 (v_{2\perp}^2 + v_{2\parallel}^2) + 2p_2 + 2B_{2\parallel}^2] v_{2\perp} - 2(v_{2\parallel} B_{2\parallel} + v_{2\perp} B_{2\perp}) B_{2\perp}$$

where the subscript "1" and "2" denote, respectively, the "upstream" and "downstream" and the subscript "$\parallel$" denotes "parallel" to the shock front.

Since it requires an enormous effort to check the shock conditions at each point of the shock front each time, and yields little significant information, we study one arbitrary section of the shock front once, i.e., at $x = 2.44$ and $T = 19.2$. Figure 13 shows the distributions of the variables along the z axis at $x = 2.44$ which are necessary to check the shock conditions; B_x and B_y are, respectively, the x and z component of the magnetic field, M and N are, respectively, the x and z components of the momentum $\rho \underset{\sim}{v}$, J is the current, ρ is the mass density, and p is the pressure. From this figure, it is evident that each variable other than the current makes a stepwise change in a narrow zone between $x \approx 0.6$ and $x \approx 0.4$ when we come down from the upstream region, namely, from $x = 1$ (the current peaks in the range of $0.4 < x < 0.6$). This indicates a strong possibility of a shock. Although there is some ambiguity in defining

the upstream and downstream values because of the finite shock width, we can reasonably define the shock layer by the area shown in Fig. 13.

The top of Table I gives the raw data of the upstream and downstream regions. In order to derive the components of normal and tangential to the shock front, we must know the angle α of the shock front measured from the x axis. Defining this angle, we can calculate the normal and tangential components from the raw data to the following relations:

$$\begin{pmatrix} A_{\parallel} \\ A_{\perp} \end{pmatrix} = \begin{pmatrix} \cos\alpha\ ,\ \sin\alpha \\ -\sin\alpha,\ \cos\alpha \end{pmatrix} \begin{pmatrix} A_x \\ A_z \end{pmatrix} \quad .$$

The best way to know the α angle is to consult the pressure contours of Fig. 12. Graphically, we can figure out that $\alpha \approx 24°$ leaving an ambiguity of a couple of degrees. The normal and tangential values transformed with $\alpha = 24°$ are given in the middle of Table I. Substituting these values into the left- and right-hand sides of the Rankine-Hugoniot relations [1]-[5], we arrive at the result given at the bottom of Table I, which shows an excellent agreement for such a finite-size shock. Judging from this excellent agreement between the upstream and downstream values, there is no doubt that the current layers observed are shock waves.

Let us then confirm that the shocks are slow. To do so, we examine the dispersion relation. The dispersion relation of the slow mode is given by

$$\frac{1}{v_{ph}^2} = \frac{V_A^2+V_s^2}{2V_A^2V_s^2\cos^2\theta}\left[1+\left(1-\frac{4V_A^2V_s^2\cos^2\theta}{(V_A^2+V_s^2)^2}\right)^{1/2}\right]$$

where v_{ph} is the phase velocity of the slow mode, V_s is the sound velocity defined by $V_s^2 = \gamma p/\rho$ ($\gamma = 2$) and θ is the angle between the normal shock and the magnetic field. From Table I, the upstream values of V_A and V_s are calculated to be $V_{A1} \approx 0.953$ and $V_{s1} \approx 0.448$. The angle θ can be determined by the relation $\theta = 90° - (\beta-\alpha)$ where β is the angle between the field line on the upstream side of the front and the x axis, which is defined by $\tan\beta = B_{1z}/B_{1x}$. Since $B_{1z}/B_{1x} \approx 0.902$ (see Table I), we obtain $\beta \approx 42°$, so that $\theta \approx 72°$. Substituting these values into the dispersion relation, we obtain $V_{ph} \approx 0.131$. Since $v_{1i} = -0.263$, the Mach number M becomes $M \approx 2$, thus indicating that the shocks are slow mode.

Before concluding this section, we remark upon another important fact, the relationship between the shock layers and the diffusion (resistive) layers. In order to clear up this question, the resistive layer is shown in Fig. 13, where the resistivity is nonzero. Evidently, the resistive layer is located well within the shock layer. This indicates that the shock is a direct consequence of the reconnection process and the resistivity acts only to inhibit the current from growing without limit.

COMPARISON BETWEEN OPEN-ENDED AND CONFINED RECONNECTIONS

Energetics

One of the most interesting aspects of the reconnection process is the energy conversion rate. Here we describe the energetics of

reconnection.

The total energy density U ($\gamma = 2$) is given by

$$U = \frac{1}{2}\rho v^2 + p + \frac{B^2}{2\mu_o} \quad . \tag{10}$$

In order to see how much magnetic energy contained in the system is converted into the plasma kinetic energy, both the total energy and magnetic energy are plotted as a function of time in Fig. 14. The solid lines represent the temporal evolutions of both the total energy and the magnetic energy for the closed boundary case (a symbol "O" is attached on the curves). The dashed lines represent the open-ended case (a symbol "x" is attached). One can recognize that the total energy for the closed case is, obviously, increasing with a linear slope after $T = 2$ at which time the total energy input flux is fixed to a constant value. The magnetic energy is also increasing monotonically. The growth rate, however, is gradually decelerated. This indicates that the plasma energy deposit in the system is accelerated as reconnection proceeds. As a result of this energy conversion from the magnetic into plasma energy, the plasma island (magnetic island) expands. In the laboratory, the plasma would result in a disruption once the island expands as far as the wall position. In space, the plasma energy would be eventually released outwards due to some instability. In the magnetotail, the energy would be released into the ionosphere along the field lines to result in an auroral breakup.

Now, let us examine the dashed curves in Fig. 14. Both energies increase initially but begin to decrease after $T \approx 13$, at which time rapid plasma acceleration starts (see Fig. 9). The fact that the

total energies decrease implies that the energy output overcomes the input. This indicates that the reconnection process acts as an active energy converter. The difference between the solid and dashed curves provides the energy released from the system by the reconnection process. From this comparison, we may conclude that a substantial amount of energy contained in the neighborhood of the X-type neutral point is converted into the plasma bulk flow energy through reconnection.

Next, we describe the details of the balance sheet of the magnetic energy. The equation describing the magnetic energy change is given by

$$\frac{\partial (B^2/2\mu_o)}{\partial t} = -\frac{1}{\mu_o}\nabla\cdot(\underset{\sim}{E}\times\underset{\sim}{B}) - \underset{\sim}{E}\cdot\underset{\sim}{j} \quad . \tag{11}$$

Integrating this equation over the rectangular box surrounded by $x = \pm 3$ yields

$$\frac{\partial}{\partial t}\int_{-3}^{3}dx\int_{-2}^{2}dz\,\frac{B^2}{2\mu_o} = \frac{2}{\mu_o}\int_{-3}^{3}dx\,(\underset{\sim}{E}\times\underset{\sim}{B})_z - \frac{2}{\mu_o}\int_{-2}^{2}dz\,(\underset{\sim}{E}\times\underset{\sim}{B})_x$$

$$- \int_{-3}^{3}dx\int_{-2}^{2}dz\,(\underset{\sim}{j}\times\underset{\sim}{B})\cdot\underset{\sim}{v} - \int_{-3}^{3}dx\int_{-2}^{2}dz\,\eta j^2 \quad . \tag{12}$$

This relation states that the balance of the magnetic energy consists of four terms. The first term on the right-hand side is the input Poynting flux through the input boundaries and the second term is the output Pynting flux through the side boundaries. The third term is the work done by the Ampere force on the plasma per unit time, which gives the plasma acceleration rate perpendicular to the mag-

the first term is the only contributor to the inflow of magnetic energy into the system. The remaining three terms provide the conversion rate of the magnetic energy into the plasma energy. As observed in the simulation runs, the plasma is markedly accelerated along the magnetic field by the pressure gradient force associated with the oblique slow shocks. This acceleration process is essential in the reconnection process, but the energy conversion by this process is not included in (12), so the conversion rate can be greater than that derived by (12).

Temporal evolutions of the four sink and source terms (absolute values) are plotted in Fig. 15 for the closed (0) and open-ended (x) processes. The upper panel corresponds to the closed case and the lower to the open-ended case. The ripples with an approximate period of $T = 4$ represent the back-and-forth plasma motion associated with the magnetosonic (fast) mode which propagates back and forth between the input boundaries. In the closed case, no output Poynting flux exists, obviously. From the upper panel, it is seen that the acceleration rate starts to increase at about $T \approx 17$. The Joule heating also arises at $T \approx 11$. These features are said to manifest the development of reconnection.

In constrast with the closed case, a drastic increase of acceleration shows up in the open-ended case. Likewise, the Joule heating and the output Poynting flux begins to increase markedly in more or less coincidence with the rapid growth of the acceleration rate. The sum of acceleration, heating, and output Poynting flux can well exceed the input Poynting flux. The decreases of the total and magnetic energies indicated in Fig. 14 are said therefore to be a

consequence of the rapid enhancement of these three terms, particularly, the increase of acceleration.

Figure 16 is similar to Fig. 15 except for case (ii). Case (ii) shows the closed system where the input flux is small, i.e., $A_o = 0.05$. As far as the energetics is concerned there appears no conspicuous signature of the onset of reconnection in this case. A magnetosonic mode steadily propagates back and forth, in spite of the fact that there arises a definite roll-up motion of the plasma inside the magnetic island [see, Fig. 7].

Some Characteristic Behaviors at Neutral Points

In the closed case, two neutral points appear: X-type and O-type. To distinguish these two points we denote them by O(x) and O(0). In the open-ended case there is the only one (X-type) neutral point, and we denote it by X(x).

Figure 17 shows the temporal evolutions of the current density at these three points. It is seen that the currents at the X-type neutral points increase until reconnection sufficiently develops ($T \lesssim 10$). Thereafter, the neutral point current for the open-ended case decreases rather rapidly, whereas the closed case decreases fairly slow. On the other hand, the current at the O-type neutral point decreases all the way and vanishes though a small oscillation remains. Of particular interest is the fact that the O-type neutral point current tends to vanish [see Drake et al., 1978; Galeev et al., 1978] but the X-type neutral point current does not, because the simple intuition coming from the local magnetic topology is reversed.

Figure 18 is the temporal evolution of the pressure. It is seen that the pressure at the X-type neutral point makes a sudden jump when the first signal of the fast mode arrives ($T \approx 2 \sim 3$). However, the pressure decreases as reconnection takes place. The decrease may be due to a fast evacuation of the accelerated plasma. In contrast with this decrease at the X point, the pressure at the O point increases continuously. In particular, after $T \approx 15$, the rate of increase is accelerated because vortices form inside the magnetic island.

Figure 19 shows the evolution of the temperature. One can find that the Joule heating takes place at the X point of the open-ended case. It is interesting, however, that the temperature at the X point of the closed case has a tendency to decrease, presumably by an adiabatic cooling. On the other hand, the temperature at the O point keeps increasing gradually owing to an adiabatic compression (we note here that no Joule heating occurs at all at the O point). Of course, the temperature distribution will differ from this if the heat conduction is included.

Finally, the evolution of the electric field is shown in Fig. 20 (no electric field at the O point). Since there is no induction field due to $\underset{\sim}{v} \times \underset{\sim}{B}$ at the neutral point, only the Ohmic electric field is shown. As can be expected from the results discussed already, the build up of the electric field is faster for the open-ended case than for the closed case.

CONCLUSIONS

We have performed numerical simulations of externally-driven 2-D magnetic reconnection for the closed- and open-ended systems.

The primary conclusions obtained by the present simulations are as follows: (1) Magnetic reconnection can indeed act as a powerful energy converter as reported by Hayashi and Sato [1978]; Sato and Hayashi [1979]; and Sato et al., [1978]. (2) Plasma acceleration takes place preferentially along the magnetic field lines of the plasma sheet boundaries for both the closed- and open-ended cases. It is shown that the acceleration is due mainly to the slow shocks that are formed along the plasma sheet boundary (somewhat inside the magnetic separatrices) [see Bratenahl and Yeates, 1970]. The perpendicular acceleration is due to the Ampere force in the slow shocks, but the stronger parallel acceleration turns out to be a result of a strong pressure gradient force along the magnetic field that obliquely intersects the shock front. (3) The shock structure is examined in detail to find that the shock jump (Rankine-Hugoniot) conditions are extremely well satisfied. It is also found that the plasma flow velocity incident on the shock front exceeds the slow mode phase velocity. Aside from the reconnection process, this simulation may be the first quantitative demonstration of slow shocks. (4) The speed of the plasma jets along the plasma sheet boundaries can reach the Alfvén speed of the upstream region for the open-ended geometry but is lower when the plasma is not free of expansion. This feature is in agreement with the experiment by Baum and Bratenahl [1977]. (5) The substantial part of the magnetic energy near the X

type neutral point is converted into the plasma kinetic energy.

ACKNOWLEDGMENTS

I wish to thank A. Pytte for his reading the manuscript.

This work is jointly supported by the United States Department of Energy Contract No. EY-76-C-02-3073 and by the Institute of Plasma Physics, Nagoya University.

TABLE I. Shock Parameters ($x = 2.44$, $T = 19\ 2$)

	ρ	p	ρv_x	ρv_z	B_x	B_z	v_x	v_z
Upstream	0.935	0.0937	-0.0824	-0.306	0.713	0.643	-0.0881	-0.327
Downstream	1.79	0.957	1.26	0.290	-0.284	0 225	0.704	0.162

	ρ	p	$\rho v_\perp$	$\rho v_\parallel$	$B_\perp$	$B_\parallel$	$v_\perp$	$v_\parallel$
Upstream	0.935	0.0937	-0 246	-0.200	0.297	0 913	-0.263	-0.214
Downstream	1.79	0.957	-0.248	1.27	0 321	-0 168	-0.139	0.709

shock condition	[1]	[2]	[3]	[4]	[5]
Upstream	-0.246	0.297	1 06	-0 176	-0 352
Downstream	-0.248	0.321	1.05	-0.205	-0 300

References

Aubry, M.P., C.T. Russell, and M.G. Kivelson, Inward motion of the magnetopause before a substorm, J. Geophys. Res., 75, 7018, 1970.

Axford, W.I., and C.O. Hines, A unifying theory of high-latitude geophysical phenomena and geomagnetic storms, Can. J. Phys., 39, 1433, 1961.

Baum, P.J., and A. Bratenahl, On reconnexion experiments and their interpretation, J. Plasma Phys., 18, 257, 1977.

Bratenahl, A., and C.M. Yeates, Experimental study of magnetic flux transfer at the hyperbolic neutral point, Phys. Fluids, 13, 2690, 1970.

Coroniti, F.V., and A. Eviator, Magnetic field reconnection in a collisionless plasma, Astrophys. J. Suppl. Ser., 33, 189, 1977.

Davidson, R.C., and N.T. Gladd, Anomalous transport properties of the lower-hybrid-drift instability, Phys. Fluids, 18, 1327, 1975.

Drake, J.F., P.L. Pritchett, and Y.C. Lee, Nonlinear evolution of tearing instabilities: violation ψ, UCLA Preprint PPG-341, 1978.

Dungey, J.W., Interplanetary magnetic field and the auroral zone, Phys. Rev. Lett., 6, 47, 1961.

Fairfield, D.H., and N.F. Ness, Configuration of the geomagnetic tail during substorms, J. Geophys. Res., 75, 7032, 1970.

Frank, L.A., K.L. Ackerson, and R.P. Lepping, On hot tenuous plasmas, fireballs, and boundary layers in the earths magnetotail, J. Geophys. Res., 81, 5859, 1976.

Galeev, A.A., F.V. Coroniti, and M. Ashour-Abdalla, Explosive tearing mode reconnection in the magnetospheric tail, Geophys. Res. Lett., 5, 707, 1978.

Hayashi, T., and T. Sato, Magnetic reconnection: Acceleration, heating and shock formation, J. Geophys. Res., 83, 217, 1978.

Hones, E.W., Jr., The magnetotail: Its generation and dissipation, in Physics of Solar Planetary Environments, edited by D.J. Williams, p 558, AGU, Washington, D.C., 1976.

Hones, E.W , Jr., Dynamics of the Magnetosphere, Astrophys. Space Lib., edited by S.-I. Akasofu, 1979.

Hones, E.W., Jr., A.T.Y. Lui, S.J. Bame and S. Singer, Prolonged tailward flow of plasmas in the thinned plasma sheet observed at $r \approx 18\ R_e$ during substorms, J. Geophys. Res., 79, 1385, 1976

Huba, J.D., N.T. Gladd, and K. Papadopoulos, The lower-hybrid-drift instability as a source of anomalous resistivity for magnetic field line reconnection, Geophys. Res. Lett., 4, 125, 19 .

Huba, J.D., N.T. Gladd, and K. Papadopoulos, Lower-hybrid-drift wave turbulence in the distant magnetosphere, J. Geophys. Res., 83, 5217, 1978.

Krimigis, S.M., and E.T. Sarris, Dynamics of the magnetosphere, Astrophys. Space Lib., edited by S.-I. Akasofu, 1979.

Lui, A.T.Y., C.-I. Meng, and S.-I. Akasofu, Search for the magnetic neutral line in the near-earth plasma sheet, J. Geophys. Res., 82, 1547, 1977.

Maezawa, K., Magnetotail boundary motion associated with geomagnetic substorms, J. Geophys. Res., 80, 3543, 1975

Nishida, A., Geomagnetic Diagnosis of the magnetosphere, Springer-Verlag, New York, 1978.

Nishida, A., and N. Nagayama, Synoptic survey for the neutral line in the magnetotail during the substorm expansion phase, J. Geophys. Res., 78, 3782, 1973.

Papadopoulos, K., Dynamics of the magnetosphere, Astrophys. Space Lib., edited by S.-I. Akasofu, 1979.

Petchek, H.E., Magnetic-field amihilation, NASA Spec. Publ. SP-50, 425, 1964.

Priest, E.R., On steady magnetic-field reconnection, Astrophys. J., 181, 227, 1973.

Pytte, T., and H.I. West, Jr., Ground-satellite correlations during substorm magnetic field configuration changes and plasma sheet thinning in the near-earth magnetotail, J. Geophys. Res. 83, 3791, 1978.

Pytte, T., R.L. McPherron, M.G. Kivelson, H.I. West, Jr., and E.W. Hones, Multiple-satellite studies of magnetospheric substorms: Radial dynamics of the plasma sheet, J. Geophys. Res., 81, 5921, 1976.

Russell, C.T., and R.L. McPherron, The magnetotail and substorms, Space Sci, Rev., 15, 205, 1973.

Sato, T., and T. Hayashi, Externally-driven magnetic reconnection and a powerful magnetic energy converter, Phys. Fluids, June issue, 1979.

Sato, T., T. Hayashi, T. Tamao, and A. Hasegawa, Confinement and jetting of plasmas by magnetic reconnection, Phys. Rev. Lett., 41, 1548, 1978.

Schindler, K., A theory of the substorm mechanism, J. Geophys. Res., 79, 2803, 1974.

Schopke, N., G. Pashmann, H. Rosenbauer, and D.H. Fairfield, Influence of the interplanetary magnetic field on the occurrence and thickness of the plasma mantle, J. Geophys. Res. 81, 2687, 1976.

Shelley, E.G., R.D. Sharp, and R.G. Johnson, He^{++} and H^{+} flux measurements in the dayside cusp: Estimates of conversion electric field J. Geophys. Res., 81, 2363, 1976.

Smith, D.F., Current instability in reconnecting current sheets, J. Geophys. Res., 82, 704, 1977.

Smith, D.F., and E.P. Priest, Current limitation in solar flares, Astrophys. J., 176, 487, 1972.

Sonnerup, B.U.O., Magnetic-field reconnexion in a highly conducting incompressible fluid, J. Plasma Phys., 4, 161, 1970.

Stern, D.P., The role of O- type neutral line in merging during substorms and solar flares, J. Geophys. Res., 84, 63, 1979.

Vasyliunas, V.M., Theoretical models of magnetic field line merging, 1, Rev. Geophys. Space Phys., 13, 303, 1975.

White, R.B., D.A. Monticello and M.N. Rosenbluth, Simulation of large magnetic islands: A possible mechanism for a major tokamak disruption, Phys. Rev. Lett., 39, 1618, 1977.

Yeh, T., and W.I. Axford, On the reconnection of magnetic field lines in conducting fluids, J. Plasma Phys., 4, 207, 1970.

Figure Captions

Fig. 1. Sketches illustrate a model of the magnetotail structure change associated with magnetic reconnection. The top sketch illustrates the normal state. The middle one illustrates a state of the magnetotail just after magnetic reconnection sets in. In this stage accelerated plasmas on the earth side of the reconnection point are still trapped and those on the antisolar side are involved in a magnetic island. The bottom sketch illustrates a stage of the substorm expansion in which stage trapped particles are precipitated down into the ionosphere and the magnetic island is propelled away tailwardly.

Fig. 2. Time series of equivector potential lines (magnetic flux surface) for the confined (closed) magnetic reconnection process [case (1)]. Note the formation and expansion of a magnetic island.

Fig. 3. Time series of plasma flow vectors corresponding to Fig. 2. Note a sudden flow pattern change between $T = 15$ and $T = 20$. In the early phase of reconnection the flow pattern shows a tearing-mode-like convection cells ($T = 5$), but as reconnection develops the flow direction suddenly reverses and the plasma is accelerated preferentially along the inner boundaries of the magnetic island (i.e., along the expanding plasma sheet boundaries). The arrow on the left shoulder of the first panel gives the Alfvén speed.

Fig. 4. Fine structure of flow pattern change between $T = 16$ and $T = 21$.

Fig. 5. Time series of 3-D displays of the pressure distribution (left column) and the current distribution (right column) for the closed

case. Note the formation of expanding 'plasma island' in the magnetic island and the formation of slow shocks along the boundaries of the plasma island.

Fig. 6. Contour maps of the pressure (top), the temperature (middle) and the density (bottom) for the confined case at T = 25 when reconnection has sufficiently developed.

Fig. 7. Formation and development of a magnetic island (left) and change of the plasma flow pattern (right) for case (ii). Note a flow pattern change similar to that seen for case (i).

Fig. 8. Formation of slow shocks (current layers) for case (ii).

Fig. 9. Time series of magnetic contour lines for the open-ended reconnection process.

Fig. 10. Time series of plasma flow vectors corresponding to Fig. 9. Note that as reconnection develops sufficiently the jet streams become more enhanced along the boundary layers of the plasma sheet (i.e., along the slow shocks). The maximum velocity reaches the Alfvén speed.

Fig. 11. Three-dimensional displays showing the formation of slow shocks (current layers) for the open-ended case.

Fig. 12. Contour maps of the pressure (top), the temperature (middle), and the density (bottom) for the open-ended case at T = 19 when reconnection has sufficiently developed. A plasma sheet with sharp boundaries is formed and rarefaction in the diffusion region occurs.

Fig. 13. A cross-sectional distribution of slow shocks.

Fig. 14. Temporal changes of the total and magnetic energies contained in the system for the confined (O) and open-ended (X) processes. The decreases of the energies after $T \approx 13$ for the open-ended process indicates that the open-ended reconnection process acts as an active magnetic energy converter.

Fig. 15. Temporal changes of the income and payment of the magnetic energy for the confined (upper) and open-ended (lower) processes. The curve designated by 'acceleration' stands for the plasma acceleration due to the Ampere force in the slow shocks. The sum of the acceleration term, Joule heating and the output Poynting flux is the payment of the magnetic energy, namely, the work done by the magnetic energy on the plasma per unit time. Note the drastic increase of the acceleration rate after $T \approx 13$ for the open-ended case, which shows a catastrophic energy conversion.

Fig. 16. Same as Fig. 13 but for case (ii) of the confined process. Note that there appears no significant indication of energy conversion for this weak injection case. The plasma is only shaken by the magnetosonic mode.

Fig. 17. Temporal evolutions of the current densities at the X and O neutral points of the closed case (solid lines) and at the X neutral point of the open-ended case (dashed line).

Fig. 18. Temporal evolutions of the pressures at the X (solid line) and O (dash and dot line) neutral points of the confined case and at the X neutral point of the open-ended case (dashed line).

Fig. 19. Temporal evolutions of the temperatures at the X (solid) and 0 (dash and dot) neutral points of the confined case and at the X neutral point of the open-ended case (dashed).

Fig. 20. Temporal evolutions of the electric fields at the X neutral points of the closed (solid line) and open-ended (dashed line) cases. Note that the electric field at the neutral point provides a good measure of the reconnection rate.

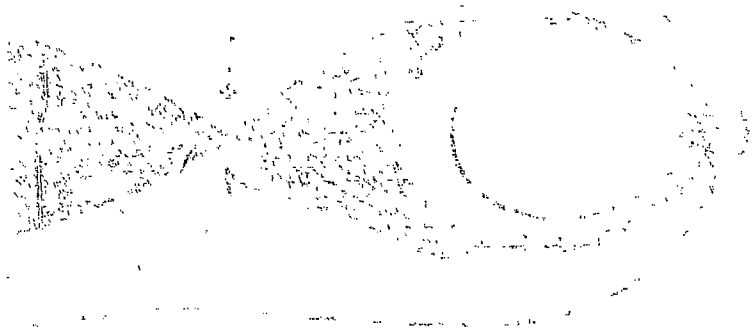

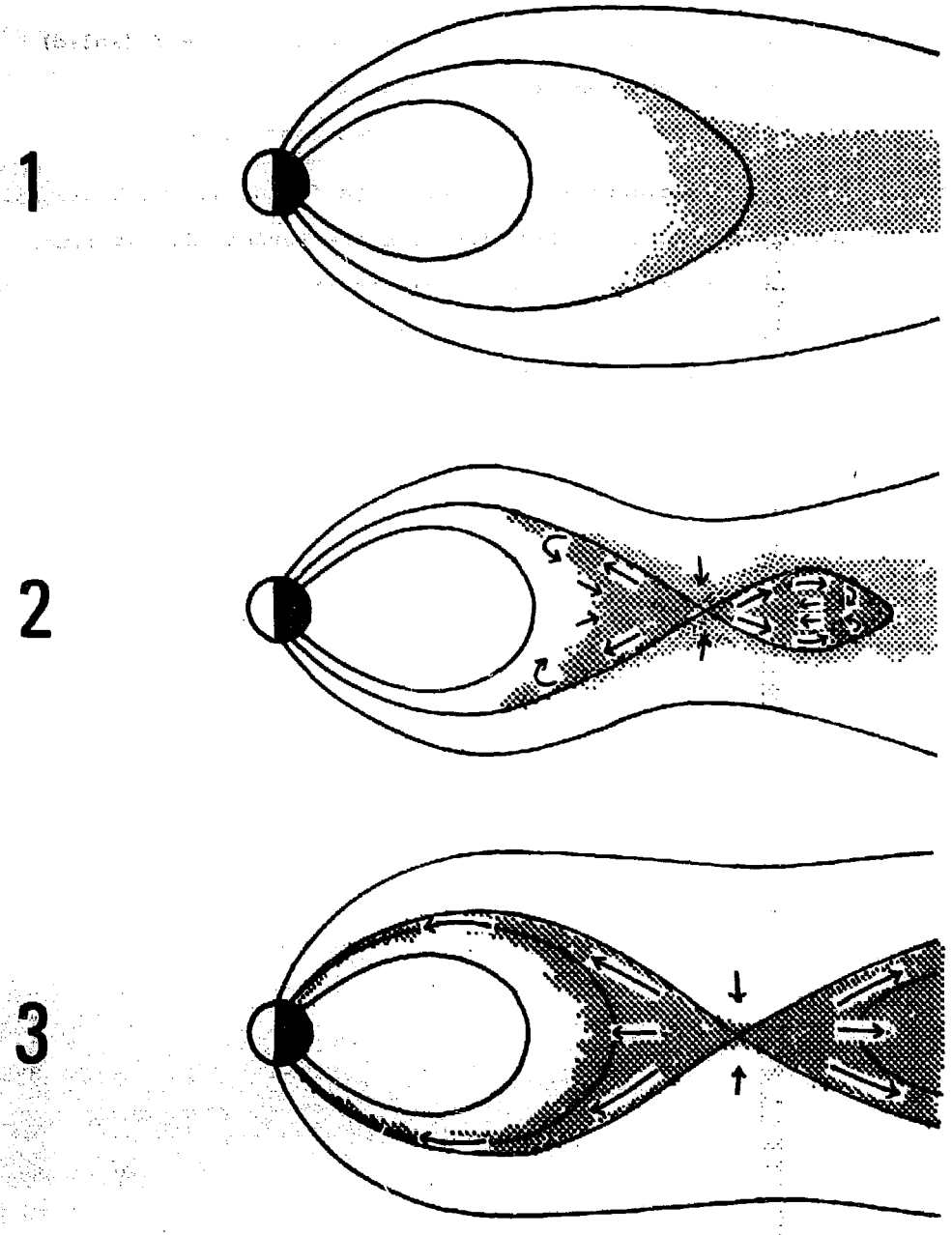

Fig. 1. 792201

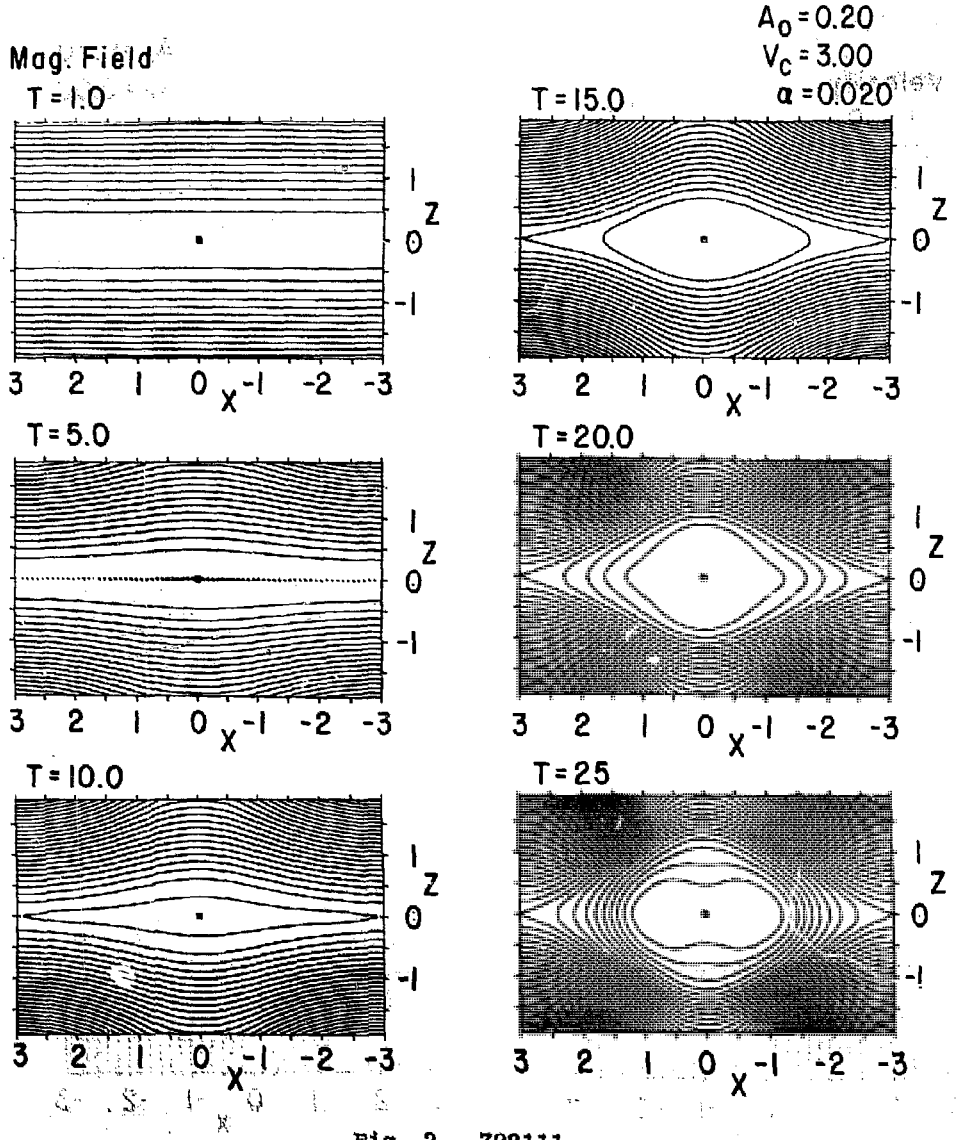
Mag. Field
$A_0 = 0.20$
$V_c = 3.00$
$\alpha = 0.020$
T = 1.0
T = 15.0
T = 5.0
T = 20.0
T = 10.0
T = 25
Z
X
1
0
-1
3 2 1 0 -1 -2 -3

Fig. 2. 792111

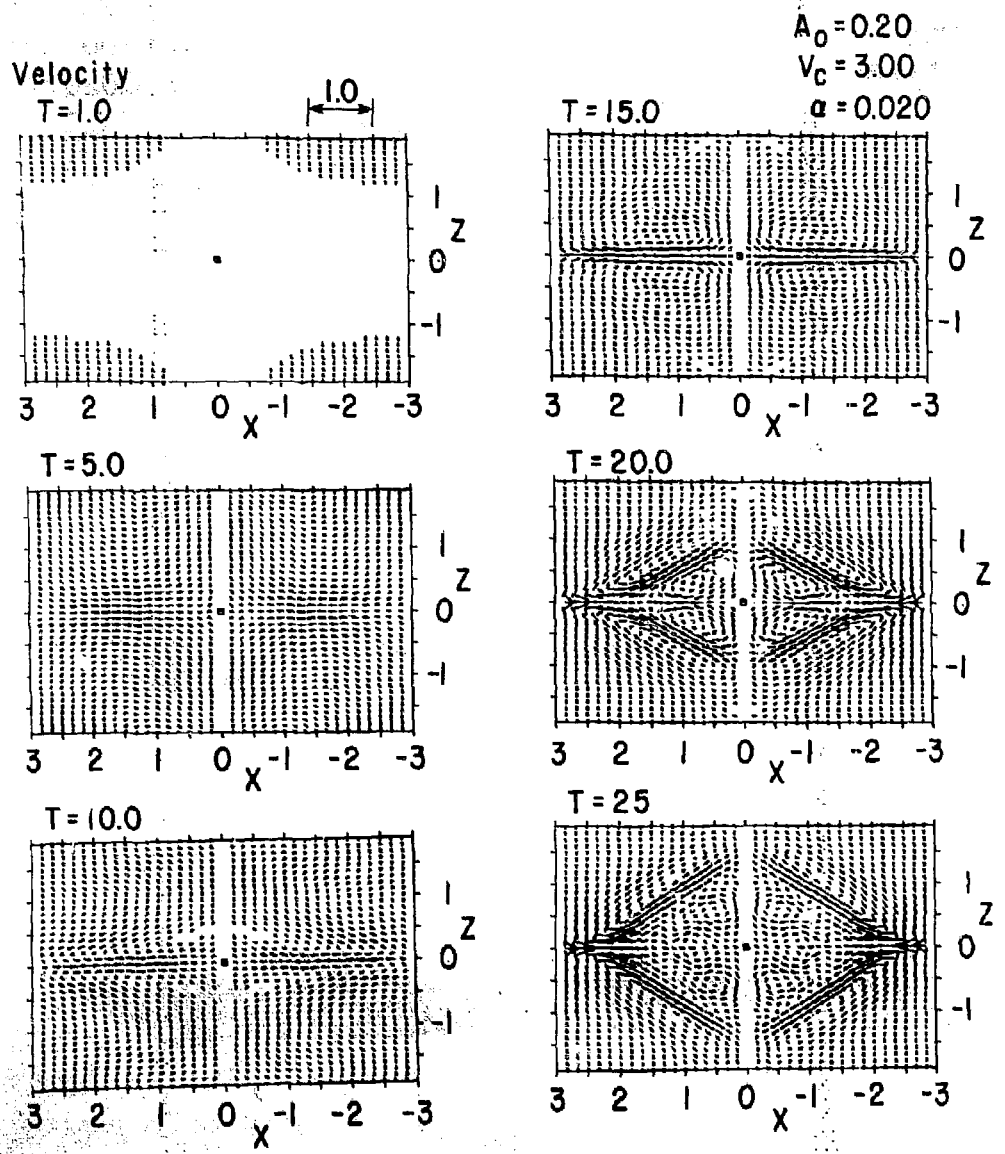
Velocity
T=1.0
1.0
T=5.0
T=10.0
T=15.0
T=20.0
T=25
$A_0 = 0.20$
$V_c = 3.00$
$\alpha = 0.020$
Z
X
3 2 1 0 -1 -2 -3
1 0 -1

Fig. 3. 792110

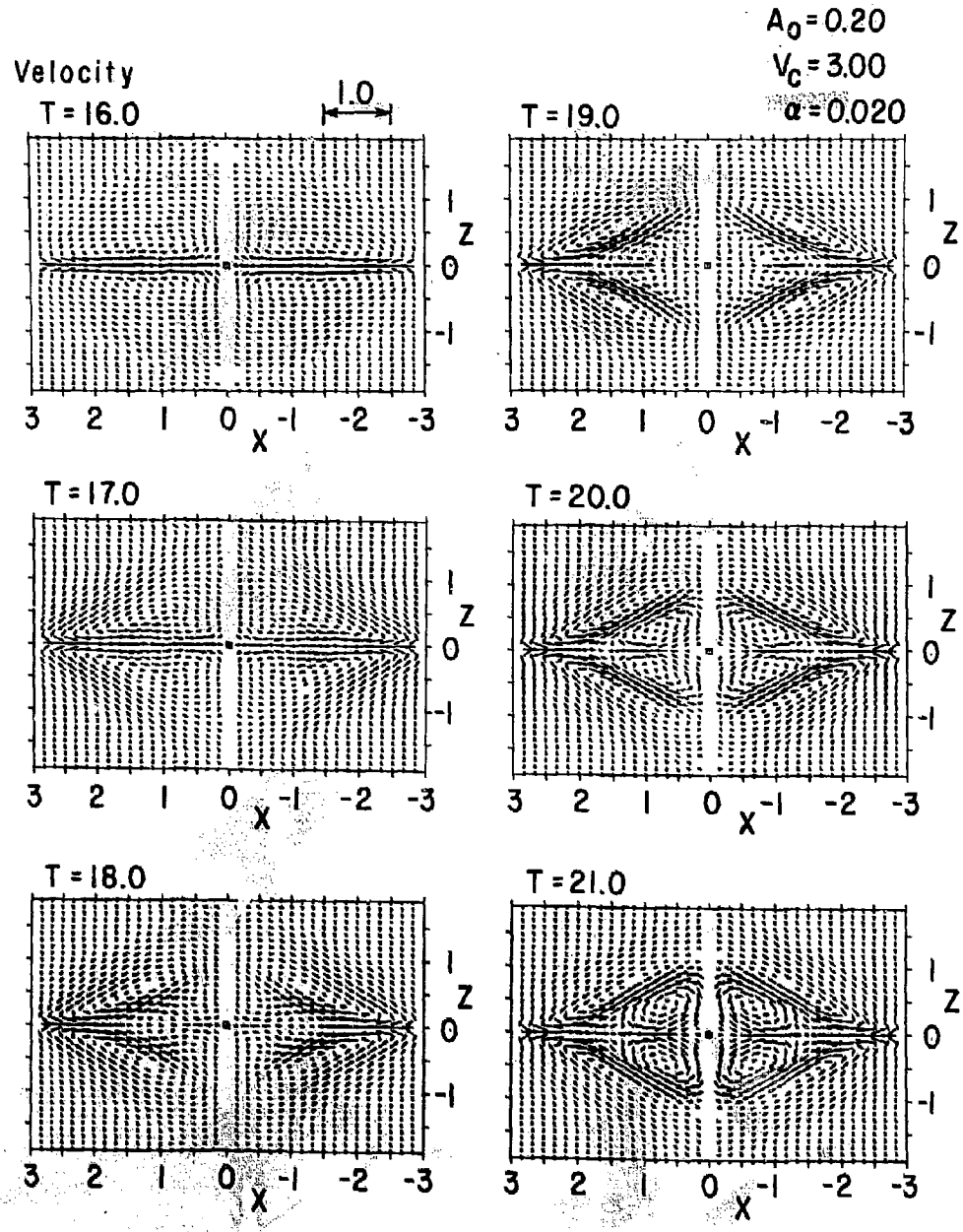
Velocity
1.0
$A_0 = 0.20$
$V_c = 3.00$
$\alpha = 0.020$
T = 16.0
T = 17.0
T = 18.0
T = 19.0
T = 20.0
T = 21.0
Z
X
3 2 1 0 -1 -2 -3
1
0
-1

Fig. 4. 792114

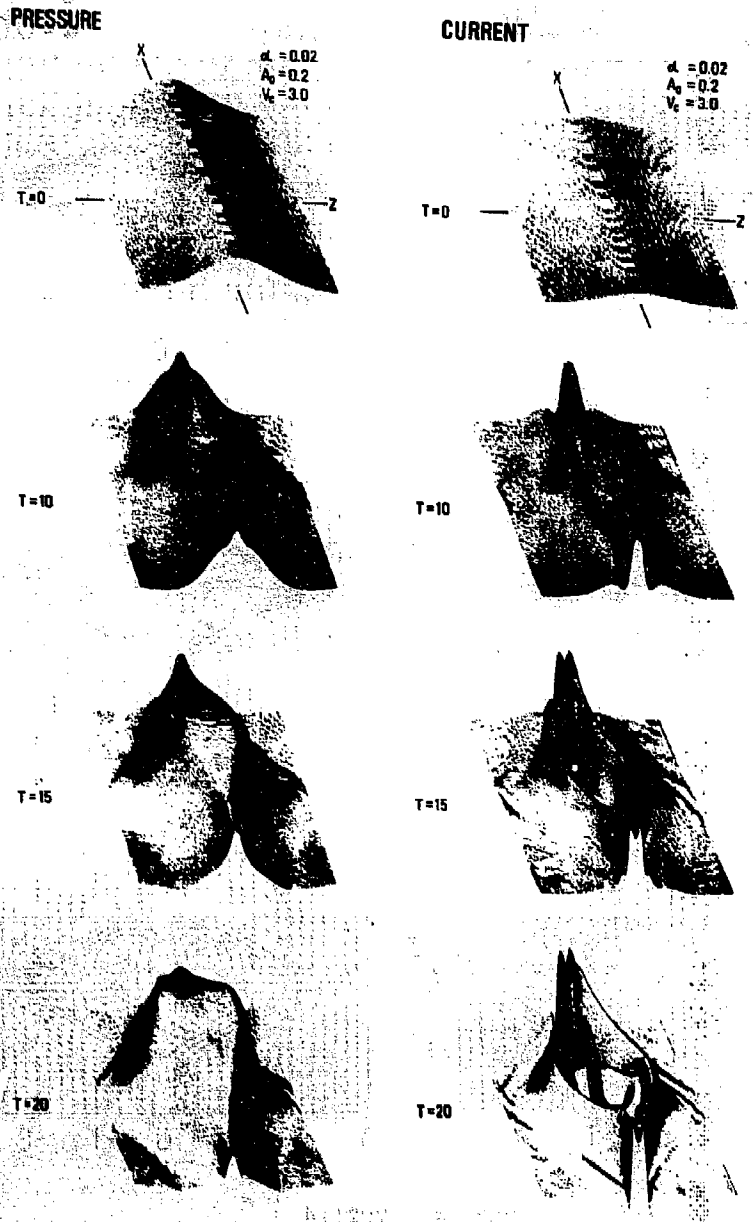

Fig. 5. 792193

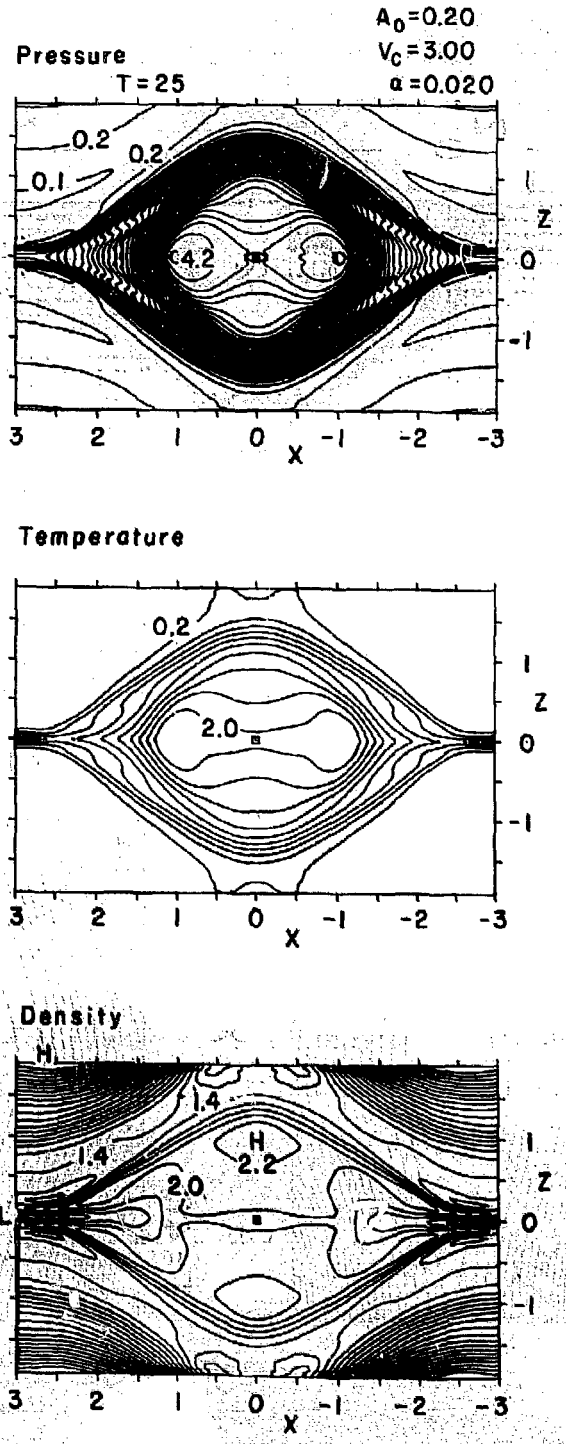
Pressure
T = 25
A_0 = 0.20
V_c = 3.00
α = 0.020
0.2
0.2
0.1
4.2
Temperature
0.2
2.0
Density
H
1.4
1.4
H
2.2
2.0
0.6
L
Z
X
3
2
1
0
-1
-2
-3

Fig. 6. 792112

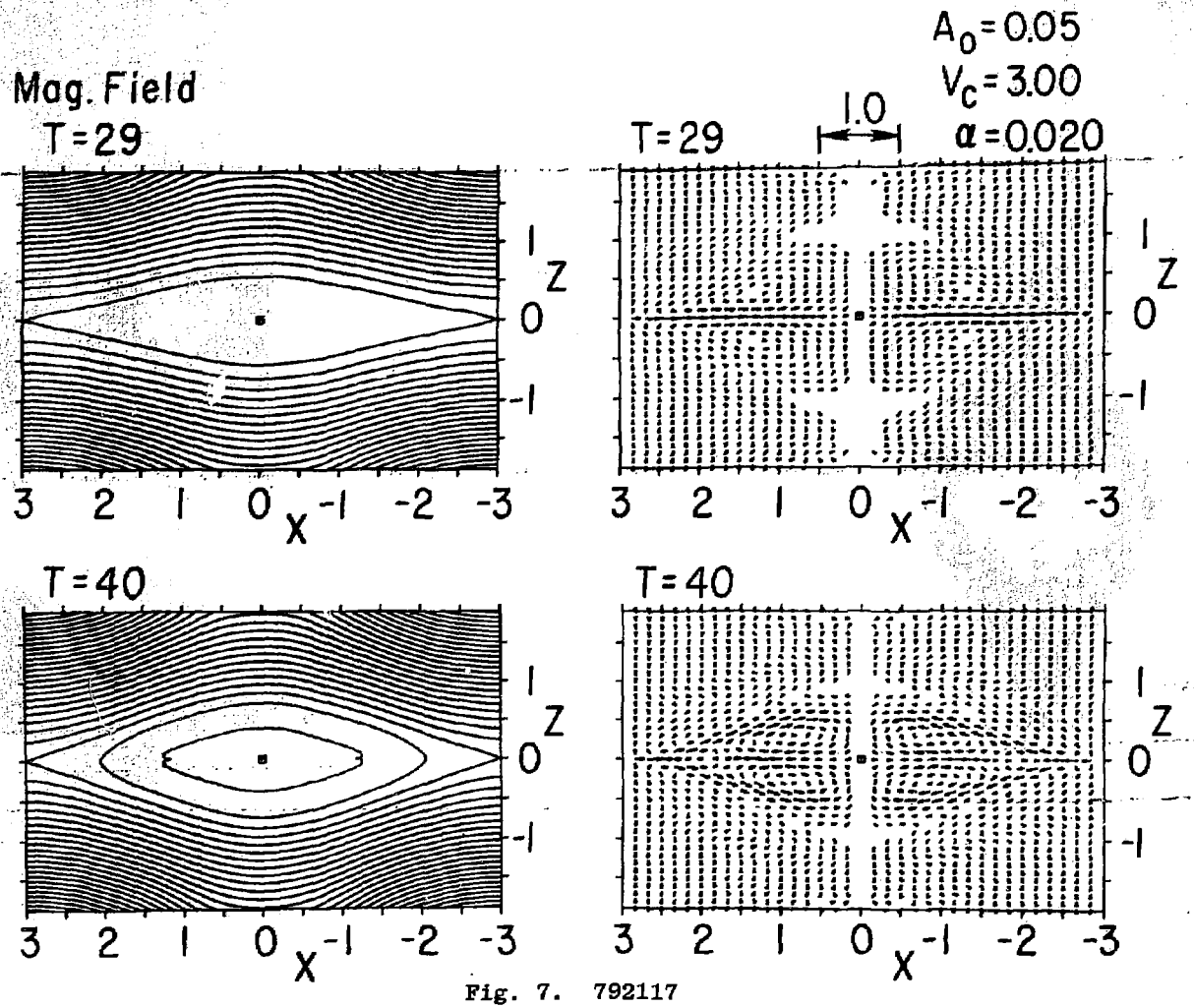

Fig. 7. 792117

CURRENT

$d = 0.02$
$A_0 = 0.05$
$V_c = 3.0$

T = 19

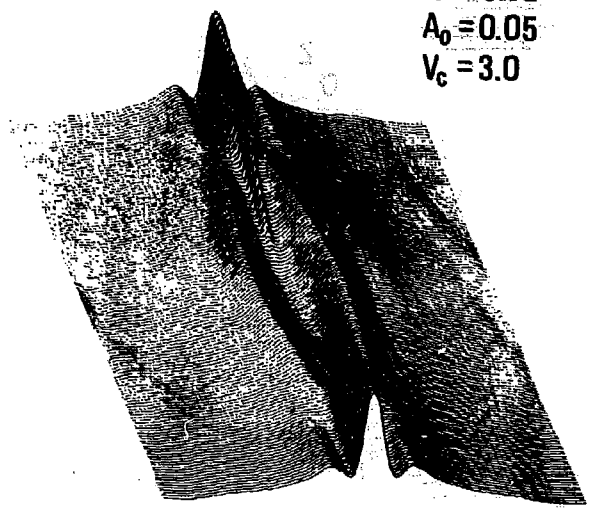

T = 39

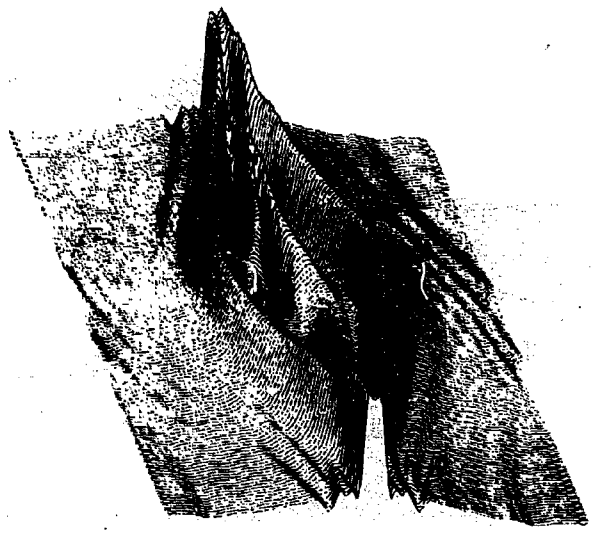

Fig. 8. 792196

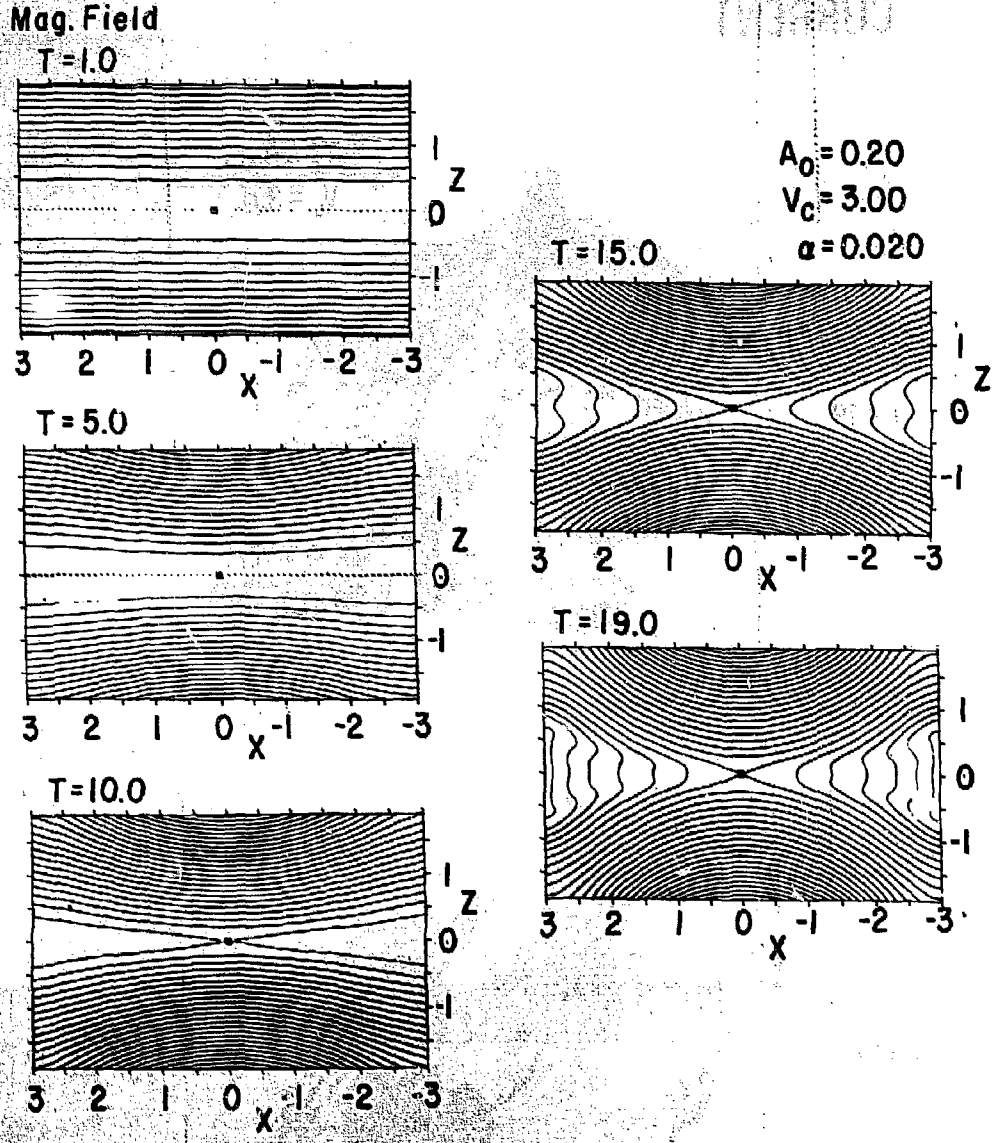
Mag. Field
T = 1.0
T = 5.0
T = 10.0
T = 15.0
T = 19.0
$A_0 = 0.20$
$V_c = 3.00$
$\alpha = 0.020$
Z
X
1
0
-1
3
2
1
0
-1
-2
-3

Fig. 9. 792118

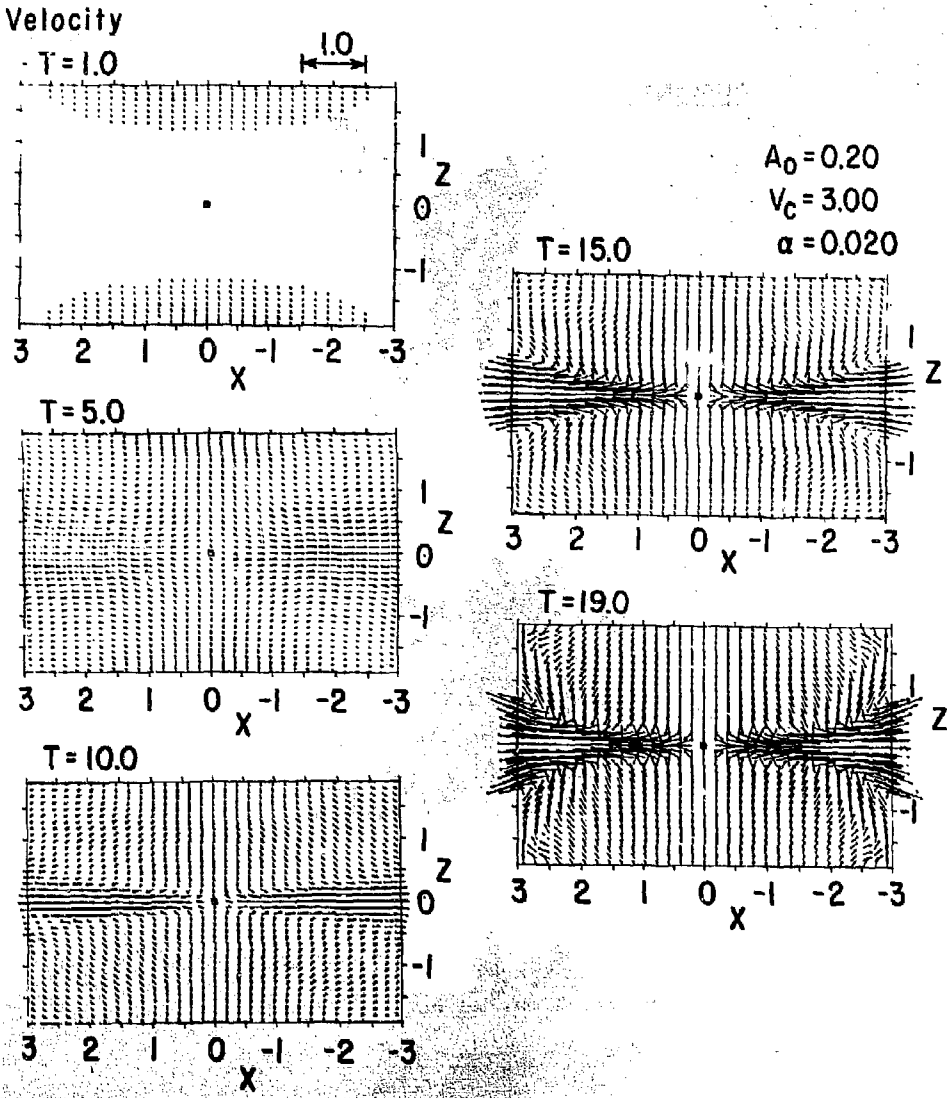

Fig. 10. 792113

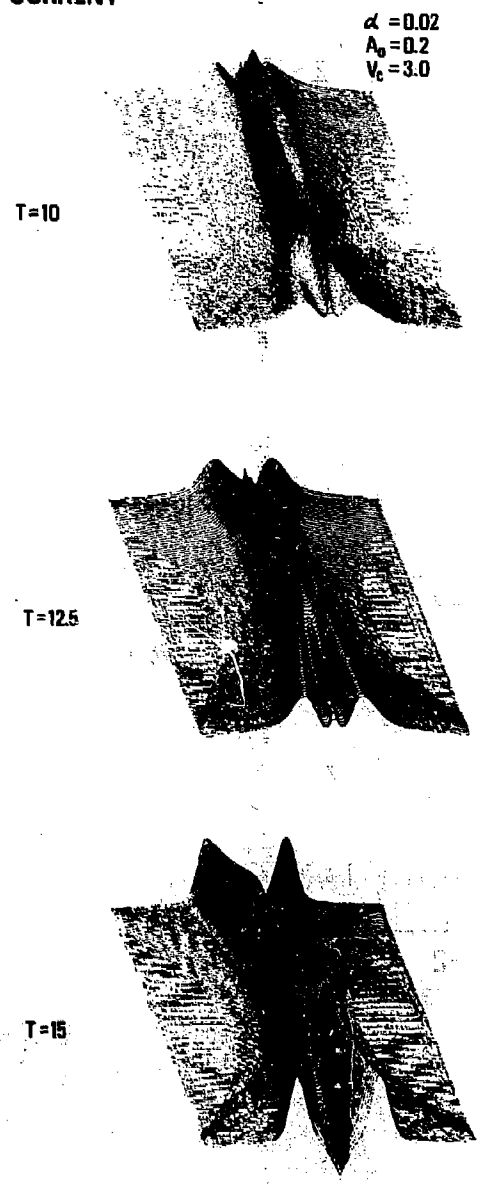

Fig. 11. 792194

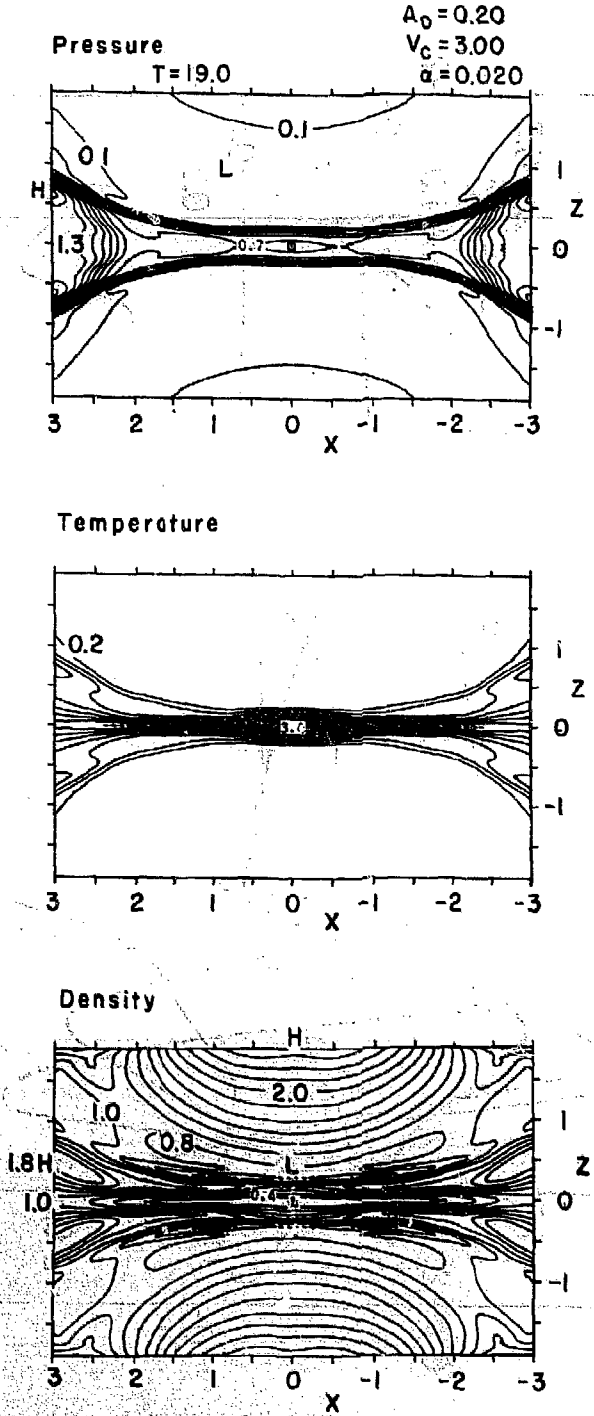

Fig. 12. 792115

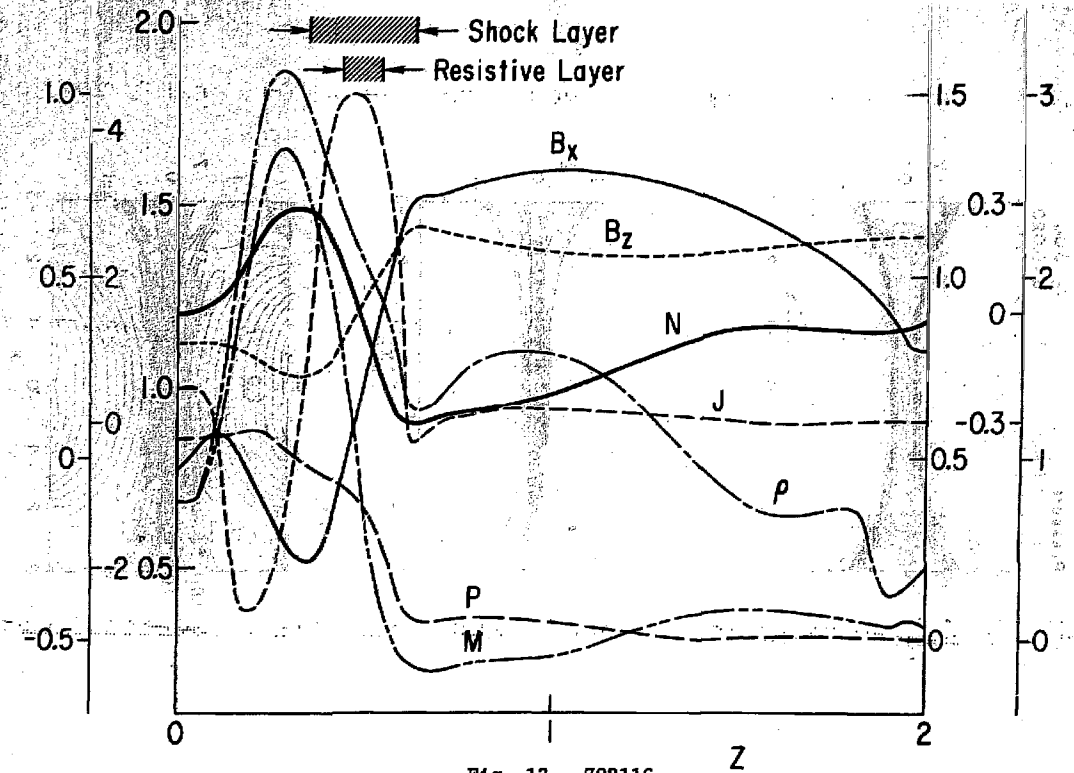

Fig. 13. 702116

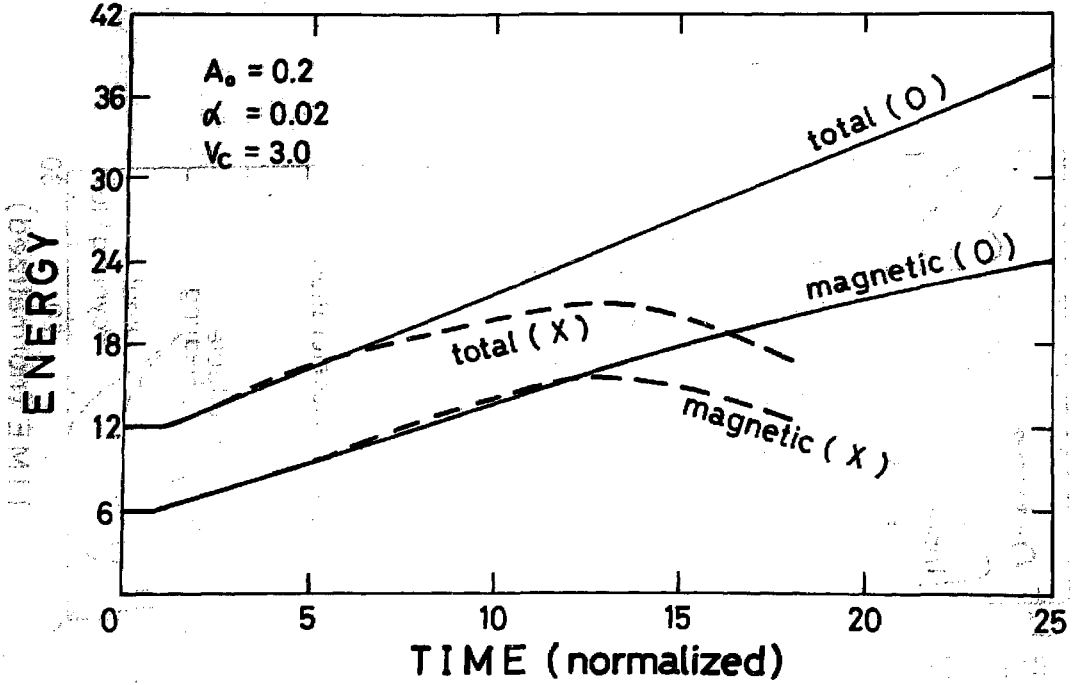

Fig. 14. 792199

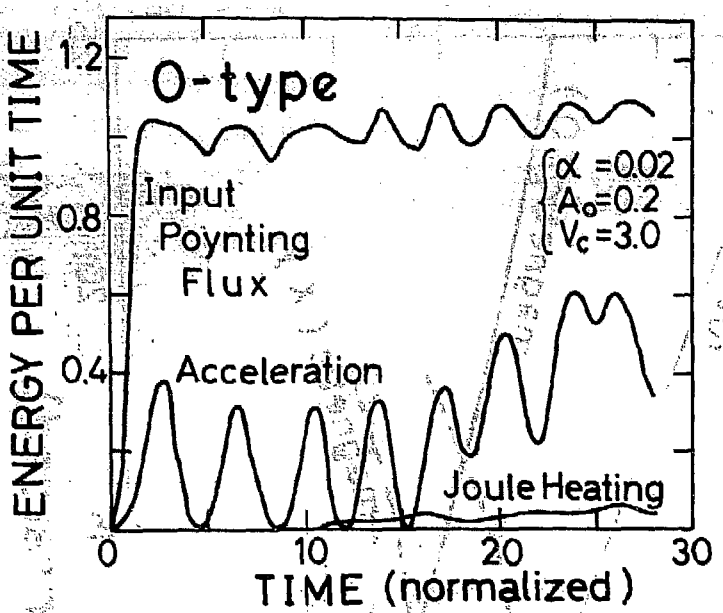

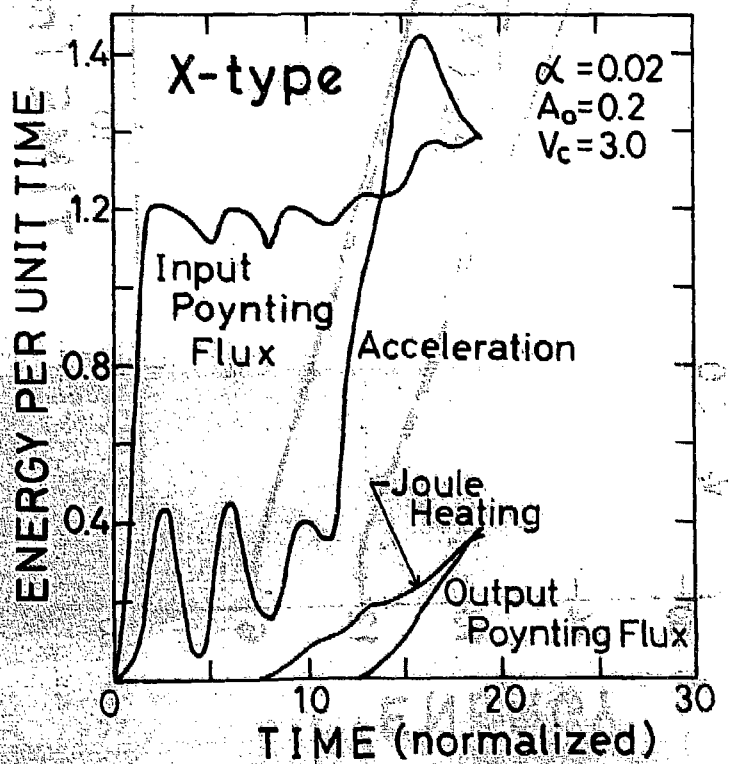

Fig. 15. 792197

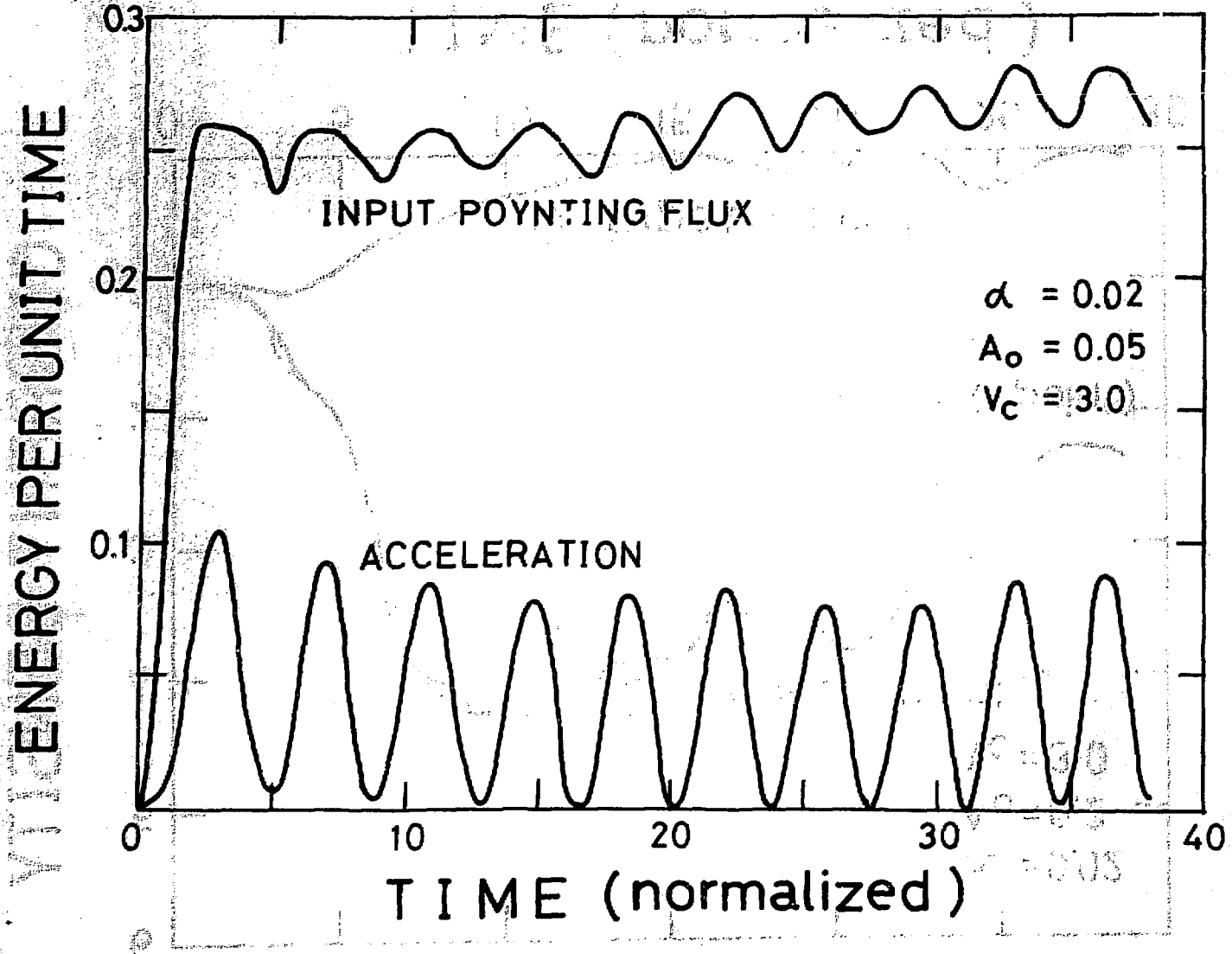

Fig. 16. 792198

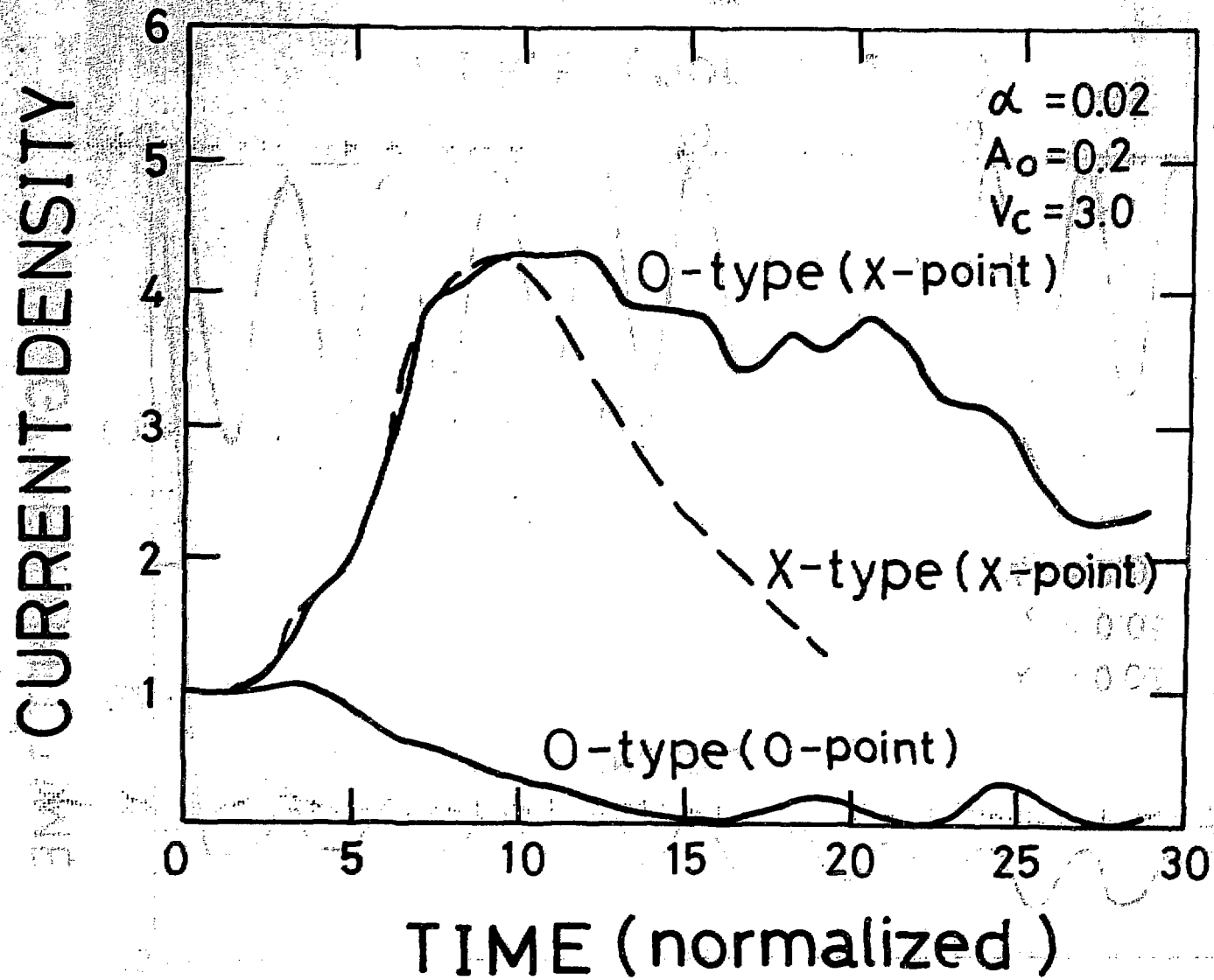

Fig. 17. 792191

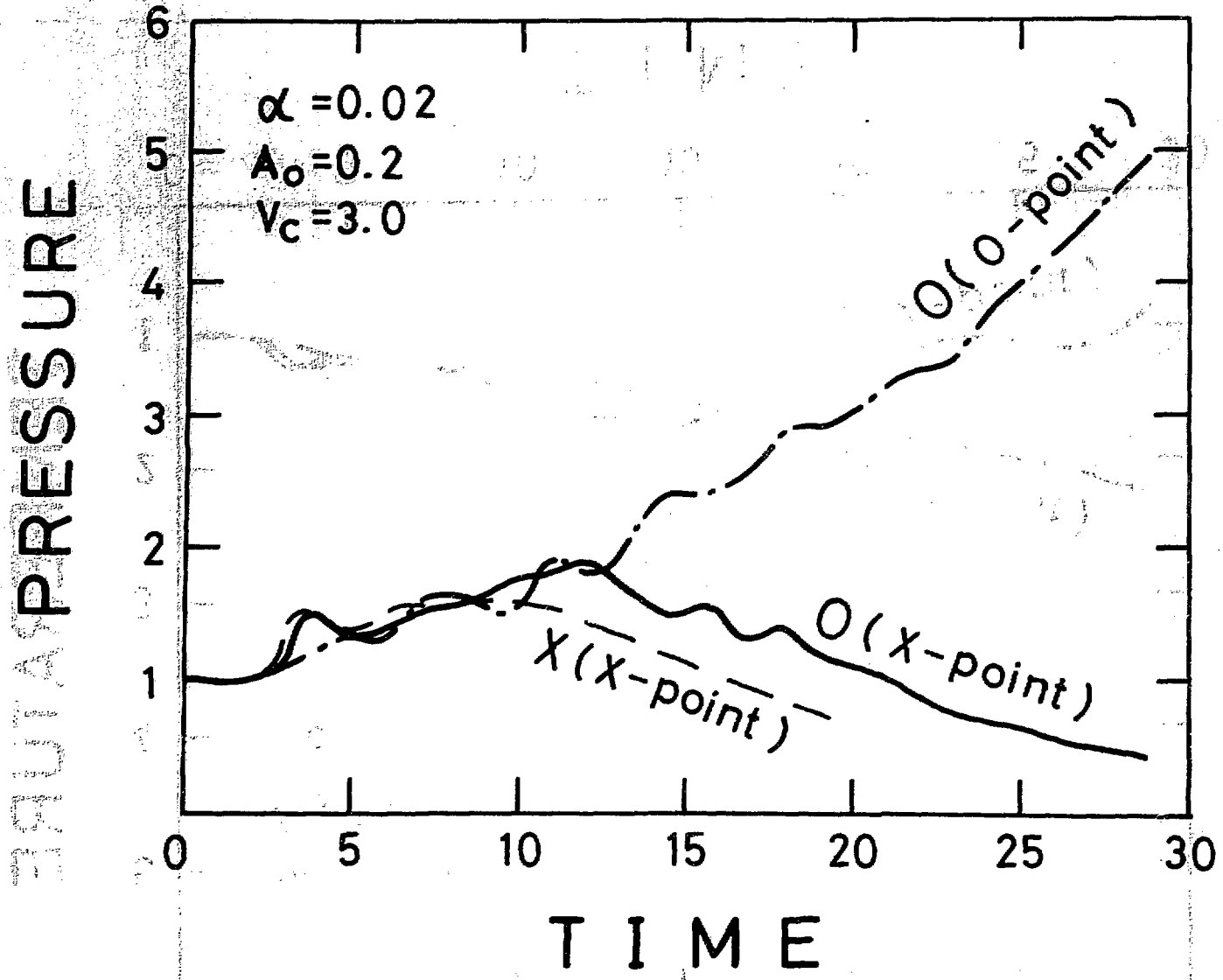

Fig. 18. 792192

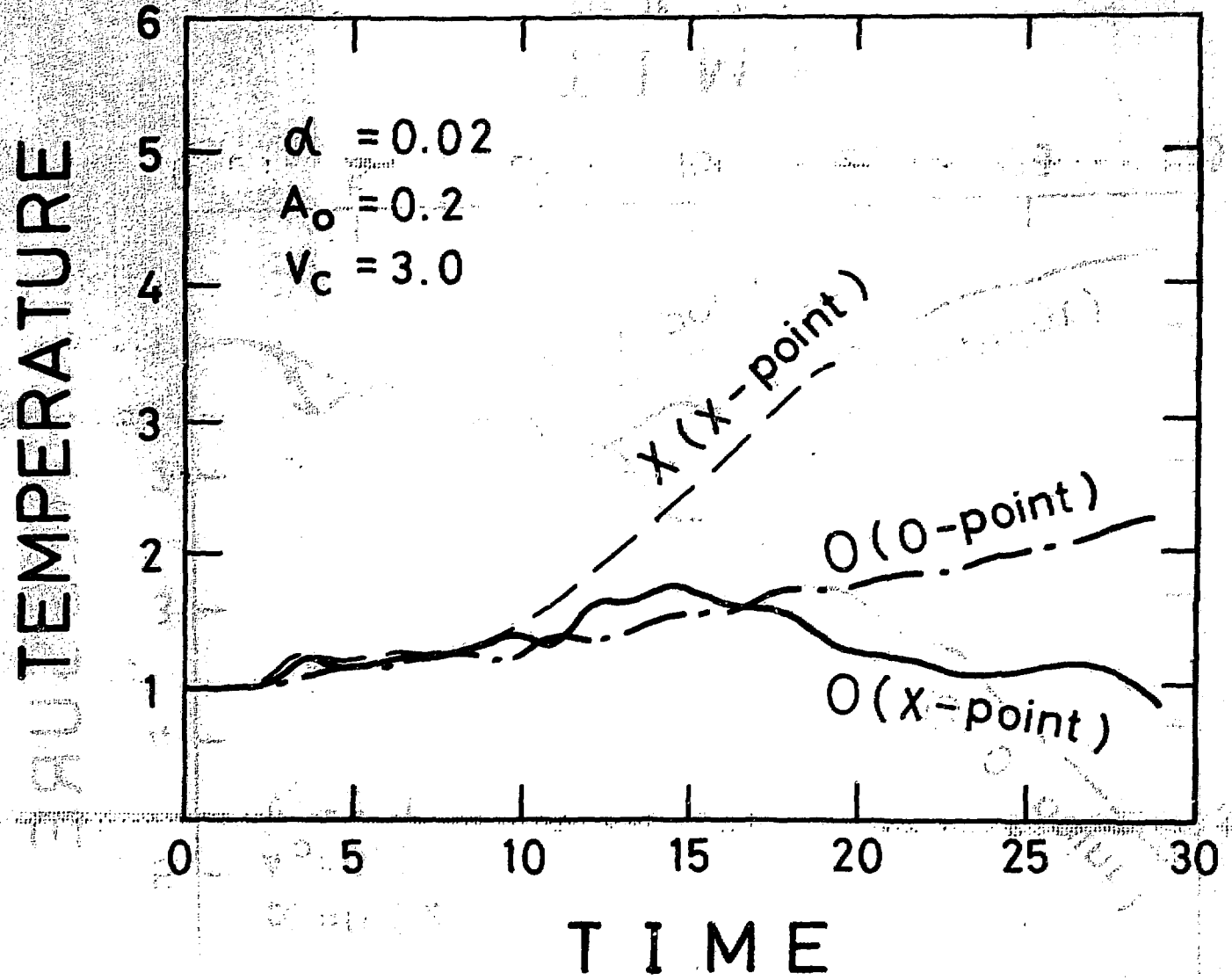

Fig. 19. 792189

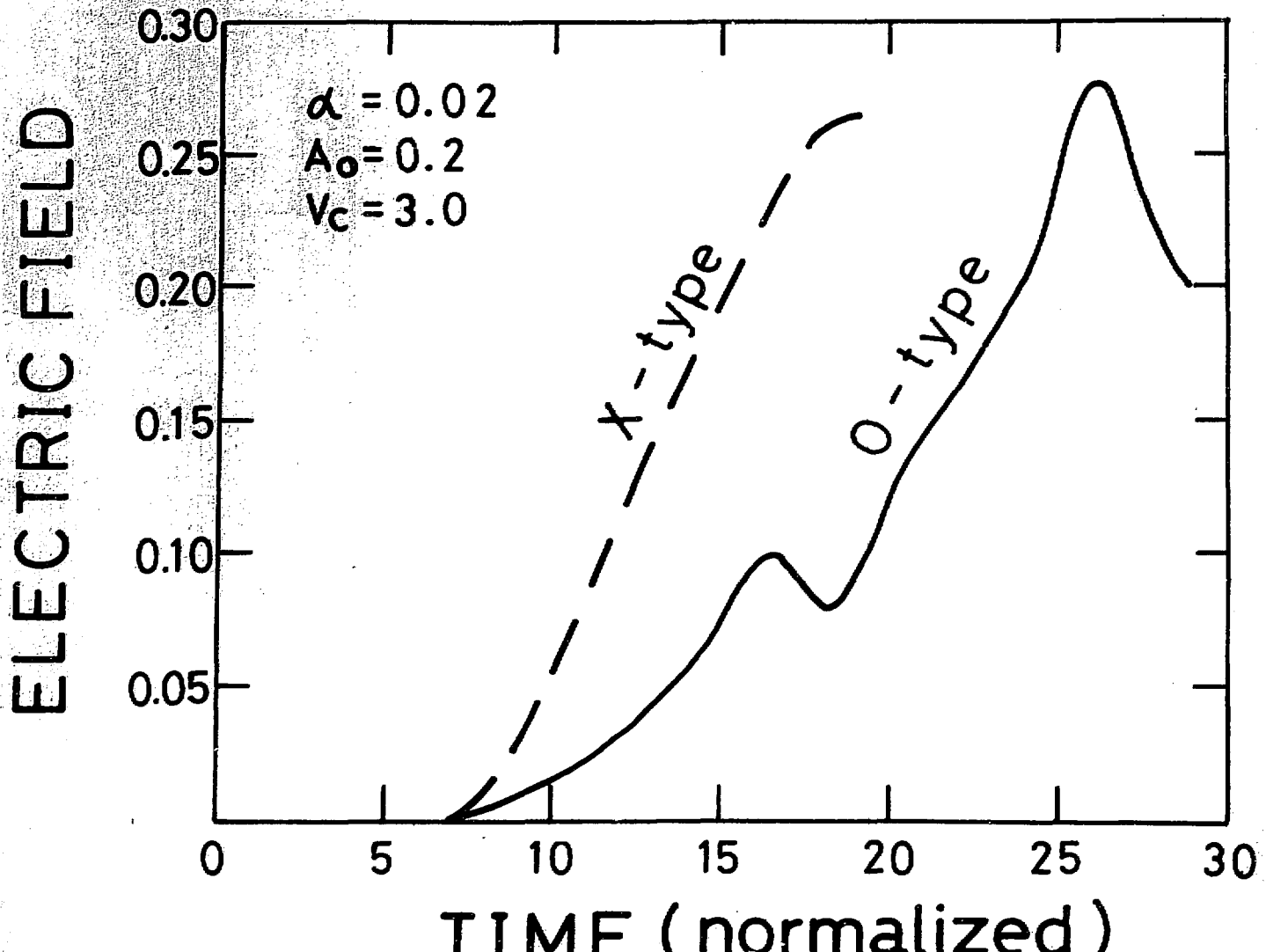

Fig. 20. 792190